iScience

CellPress
OPEN ACCESS

Article

CircPOFUT1 fosters colorectal cancer metastasis and chemoresistance via decoying miR-653-5p/E2F7/WDR66 axis and stabilizing BMI1

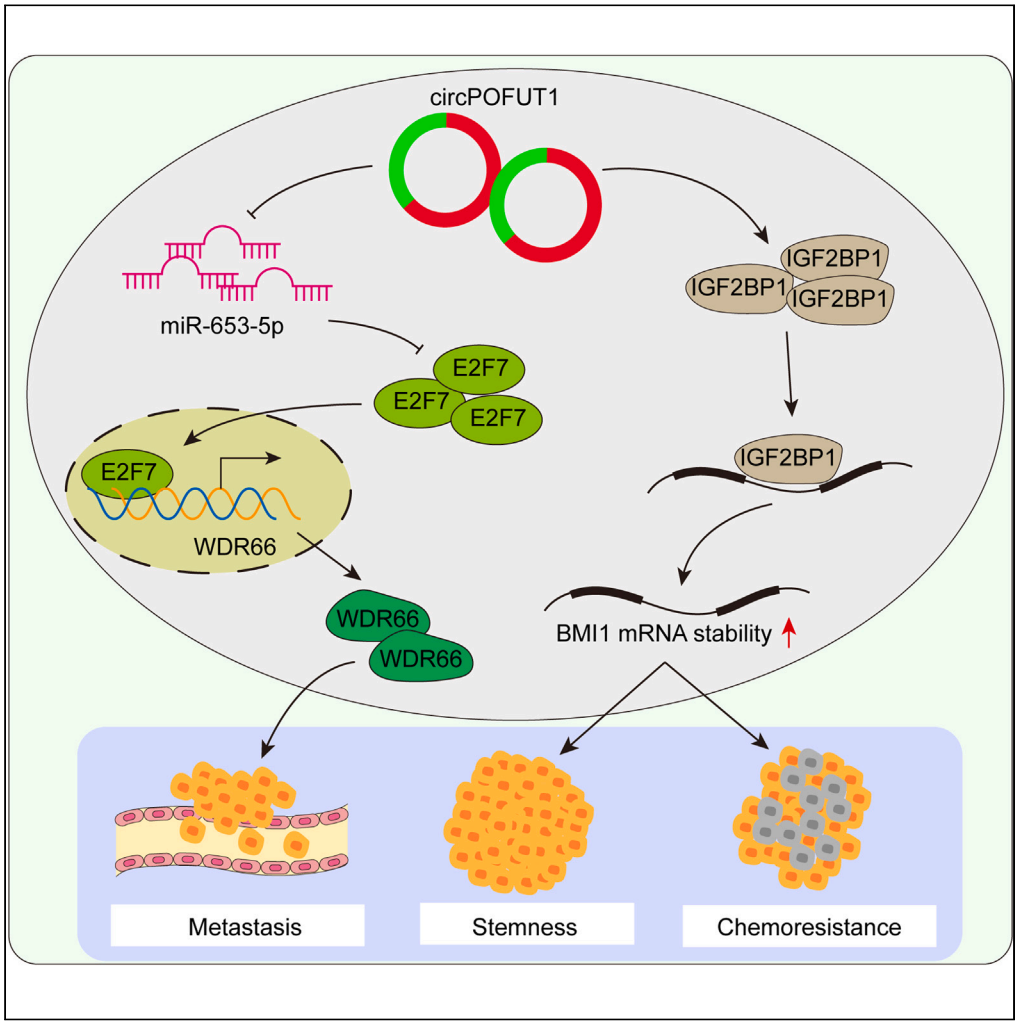

Fei Long, Buning Tian, Liang Li, ..., Yihang Guo, Miao Chen, Gui Hu

hugui22@csu.edu.cn

Highlights

CircPOFUT1 was highly expressed in CRC tissues and facilitated CRC progression

CircPOFUT1 regulated the function of E2F7 via sponging miR-653-5p

WDR66 was a downstream effector of E2F7 in circPOFUT1-mediated CRC metastasis

CircPOFUT1 promoted stemness and chemoresistance of CRC cells via stabilizing BMI1

Long et al., iScience *27*, 108729
January 19, 2024
https://doi.org/10.1016/j.isci.2023.108729

iScience

CellPress
OPEN ACCESS

Article

CircPOFUT1 fosters colorectal cancer metastasis and chemoresistance via decoying miR-653-5p/E2F7/WDR66 axis and stabilizing BMI1

Fei Long,[1,2,3] Buning Tian,[1,3] Liang Li,[1] Min Ma,[1] Zhijian Chen,[1] Guojiang Tan,[1] Ning Yin,[1] Chonglei Zhong,[1] Bowen Yu,[1] Yihang Guo,[1] Miao Chen,[1] and Gui Hu[1,4,*]

SUMMARY

CircRNAs are implicated in colorectal cancer (CRC) development and progression. Protein O-fucosyltransferase 1 (POFUT1) plays an oncogenic role via activating Notch1 signaling in CRC. However, the roles of circPOFUT1, which is originated from POFUT1, have not been investigated. Our study showed circPOFUT1 was highly expressed in CRC tissues and cells. CircPOFUT1 enhanced the proliferation, migration and invasion of CRC cells, and promoted tumor growth and liver metastasis *in vivo*. It also reinforced stemness and chemoresistance of CRC cells. Mechanistically, circPOFUT1 regulated the function of E2F7 via sponging miR-653-5p, thereby transcriptionally inducing WDR66 expression and further promoting metastasis in CRC. On the other hand, circPOFUT1 promoted stemness and chemoresistance of CRC cells via stabilizing BMI1 in an IGF2BP1-dependent manner. In conclusion, circPOFUT1 fosters CRC metastasis and chemoresistance via decoying miR-653-5p/E2F7/WDR66 axis and stabilizing BMI1.

INTRODUCTION

Colorectal cancer (CRC) is the third frequently diagnosed cancer worldwide.[1] In recent years, incidence declines in adults aged >65 years, but rising incidence has been found in young and middle-aged adults.[1,2] Despite advances in diagnostic and therapeutic strategies, the prognosis of CRC remains unfavorable due to late-stage diagnosis, chemoresistance, metastasis and relapse.[3] Identification of biological markers and elucidation of underlying mechanism may provide promising insight into CRC diagnosis and treatment.

Chemotherapy remains the first-line therapy for CRC. Unfortunately, patients with CRC frequently develop chemoresistance, which is associated with dismal prognosis.[4] Growing evidence indicates that cancer stem cells (CSCs) which exhibited stem cell-like features have been identified in a variety of cancers, and implicated in CRC progression, metastasis and chemoresistance.[5,6] Chemoresistance can be inherent or/and acquired.[7] Elevated expression of ATP-binding cassette transporters is found in CSCs, which contributes to drug efflux, leading to inherent resistance.[7,8] CSCs survived chemotherapy may accumulate mutations to acquire chemoresistance.[9] Gaining a better understanding of mechanism underlying stemness and chemoresistance in CRC might achieve improved clinical outcomes.

Circular RNAs (circRNAs) are a class of single-stranded RNAs with closed loop structure.[10,11] Given their unique ring structure without free 3′ or 5′ end, circRNAs are more stable and conserved.[12] In recent years, emerging evidence indicates the functions of circRNAs, including serving as miRNA sponges, regulating transcription via recruitment of transcription factor, as well as ability for translation.[13–15] More importantly, it has been reported that circRNAs are implicated in cell proliferation, apoptosis, metastasis and drug resistance in CRC,[16] suggesting the potential of circRNAs in the diagnosis and treatment of CRC. Our previous study has demonstrated that protein O-fucosyltransferase 1 (POFUT1) plays an oncogenic role via activating Notch1 signaling in CRC.[17] However, the functions of circPOFUT1 (hsa_circ_0059774, originated from POFUT1 pre-mRNA) in CRC remain elusive.

In this study, we demonstrated that circPOFUT1 was highly expressed in CRC tissues and cells. CircPOFUT1 enhanced cell proliferation, migration, and invasion *in vitro* and induced liver metastasis *in vivo*. It also reinforced stemness and chemoresistance of CRC cells. Mechanistically, circPOFUT1 regulated the function of E2F7 via sponging miR-653-5p, thereby transcriptionally inducing WDR66 expression and further promoting metastasis in CRC. On the other hand, circPOFUT1 promoted stemness and chemoresistance of CRC cells via stabilizing BMI1 in a IGF2BP1-dependent manner. These findings provided in-depth insights into the diagnosis and treatment of CRC.

[1]Department of Gastrointestinal Surgery, The Third Xiangya Hospital, Central South University, Changsha, Hunan 410013, China
[2]Postdoctoral Station of Basic Medicine, The Third Xiangya Hospital, Central South University, Changsha, Hunan 410013, China
[3]These authors contributed equally
[4]Lead contact
*Correspondence: hugui22@csu.edu.cn
https://doi.org/10.1016/j.isci.2023.108729

RESULTS

CircPOFUT1 is highly expressed in colorectal cancer tissues and cells

CircPOFUT1 is originated from POFUT1 pre-mRNA based on UCSC (Figure 1A). It is originated from exons 3 and 4 of the POFUT1 pre-mRNA (Figure 1B). As shown in Figures 1C and 1D, circPOFUT1 was much more stable than POFUT1 mRNA in which the POFUT1 mRNA level was significantly decreased upon RNase R or actinomycin D treatment in SW480 cells. To further explore the biological roles of circPOFUT1 in CRC, the circPOFUT1 expression level was examined in clinical specimens. qRT-PCR showed that circPOFUT1 was elevated in CRC tissues (Figure 1E and Table 1). It was remarkably upregulated in stage II and stage III+IV CRC tissues compared with stage I CRC tissues, suggesting that circPOFUT1 level was positively correlated with TNM stage (Figure 1F). In addition, Kaplan-Meier analysis revealed that patients with CRC with high circPOFUT1 level exhibited poor overall survival in comparison with those with low circPOFUT1 level (Figure 1G), indicating that high circPOFUT1 level was associated with poor prognosis in CRC. Moreover, circPOFUT1 was markedly elevated in CRC cell lines LoVo, HT29, HCT116, SW480 and SW620 cells, compared with normal colon cell line FHC cells (Figure 1H). HCT116 cells with relatively low circPOFUT1 expression level and SW480 cells with relatively high circPOFUT1 expression level were selected for subsequent experiments. Subcellular fractionation coupled with qRT-PCR showed that circPOFUT1 was detected in both nuclei and cytoplasm, and it was predominantly expressed in the cytoplasm of HCT116 and SW480 cells (Figure 1I). This finding was further validated by FISH assay (Figure 1J). Collectively, these data suggest that circPOFUT1 is upregulated in CRC tissues and cells, and it is positively correlated with TNM stage and poor overall survival in patients with CRC.

CircPOFUT1 enhances cell proliferation, migration and invasion *in vitro* and induces tumor growth and liver metastasis *in vivo*

Gain- and loss-of function experiments were next performed to study the functions of circPOFUT1 in CRC cells. As presented in Figure 2A, lentiviral vectors including sh-circPOFUT1#1 and sh-circPOFUT1#2 successfully decreased circPOFUT1 expression in SW480 cells. By contrast, lentivirus-mediated overexpression of circPOFUT1 markedly induced circPOFUT1 expression in HCT116 cells. CCK-8 assay showed that silencing of circPOFUT1 inhibited cell proliferation in SW480 cells, while overexpression of circPOFUT1 exerted an opposite effect on cell proliferation in HCT116 cells (Figure 2B). Consistently, EdU incorporation and colony formation assays further revealed that the proliferative capacities of SW480 cells were impaired by circPOFUT1 knockdown, whereas circPOFUT1 overexpression promoted cell proliferation in HCT116 cells (Figures 2C and 2D). As presented in Figure 2E, silencing of circPOFUT1 decreased tumor volume and weight, whereas circPOFUT1 overexpression promoted tumor growth *in vivo*. In addition, knockdown of circPOFUT1 inhibited cell migration and invasion in SW480 cells, while the migratory and invasive capabilities of HCT116 cells were enhanced by circPOFUT1 overexpression (Figure 3A). In line with these findings, the upregulation of epithelial marker E-cadherin, along with the downregulation of mesenchymal markers N-cadherin and vimentin were observed in circPOFUT1-knockdown SW480 cells. Opposite expression patterns of these epithelial-mesenchymal transition (EMT) markers were found in circPOFUT1-overexpressing HCT116 cells as detected by immunofluorescence and Western blot assays (Figures 3B and 3C), indicating that circPOFUT1 promoted EMT in CRC cells. Furthermore, silencing of circPOFUT1 decreased the number of metastatic nodules in liver tissues in the tail-vein injection xenograft model (Figures 3D–3F). To further validate the metastatic effects caused by circPOFUT1, the hepatic metastatic xenograft model was established by intrasplenic injection. In this model, knockdown of circPOFUT1 also suppressed liver metastasis in which the hepatic metastatic nodules were remarkably decreased in circPOFUT1-knockdown group (Figures 3G–3I). Taken together, these findings suggest that circPOFUT1 enhances cell proliferation, migration and invasion *in vitro* and induces liver metastasis *in vivo*.

CircPOFUT1 reinforces stem cell-like properties and chemoresistance of colorectal cancer cells

We next examined the effects of circPOFUT1 on stem cell-like properties and chemoresistance of CRC cells. Sphere formation assay further showed that knockdown of circPOFUT1 significantly impaired the sphere formation abilities of SW480 cells, whereas circPOFUT1 overexpression promoted sphere formation in HCT116 cells (Figure 4A). Consistently, the stemness-related markers CD133, SOX2 and CD44 were downregulated in circPOFUT1-knockdown SW480 cells, while these markers were upregulated in circPOFUT1-overexpressing HCT116 cells (Figure 4B). In order to investigate the roles of circPOFUT1 on chemoresistance, transfected CRC cells were treated with different doses of 5-fluorouracil (5-Fu). CCK-8 assay revealed that silencing of circPOFUT1 enhanced the sensitivity of SW480 cells to 5-Fu, while circPOFUT1 overexpression exerted an opposite effect on the sensitivity to 5-Fu in HCT116 cells (Figure 4C). Moreover, 5-Fu-induced apoptosis was potentiated by sh-circPOFUT1 in SW480 cells, whereas OE-circPOFUT1 attenuated 5-Fu-induced apoptosis in HCT116 cells as detected by Annexin-V-FITC/PI staining (Figure 4D). Together, these data indicate that circPOFUT1 reinforces stem cell-like properties and chemoresistance of CRC cells.

CircPOFUT1 serves as a sponge of miR-653-5p

In order to unravel the downstream signaling of circPOFUT1, five putative miRNAs with high matching scores were predicted using Starbase and Circinteractome, including miR-1197, miR-1252-5p, miR-136-5p, miR-149-5p and miR-653-5p (Figure 5A). RNA pull-down assays were performed to verify the circPOFUT1/miRNAs interaction. As shown in Figure 5B, biotinylated circPOFUT1 successfully pulled down itself, suggesting the specificity of circPOFUT1 probe. Interestingly, miR-1197, miR-1252-5p and miR-653-5p were pulled down by circPOFUT1 in SW480 cells, and miR-149-5p and miR-653-5p were enriched by circPOFUT1 in HCT116 cells (Figure 5C). Given the verified interaction between circPOFUT1 and miR-653-5p in both CRC cells, we next focused on miR-653-5p in the subsequent experiments. As expected, biotinylated miR-653-5p

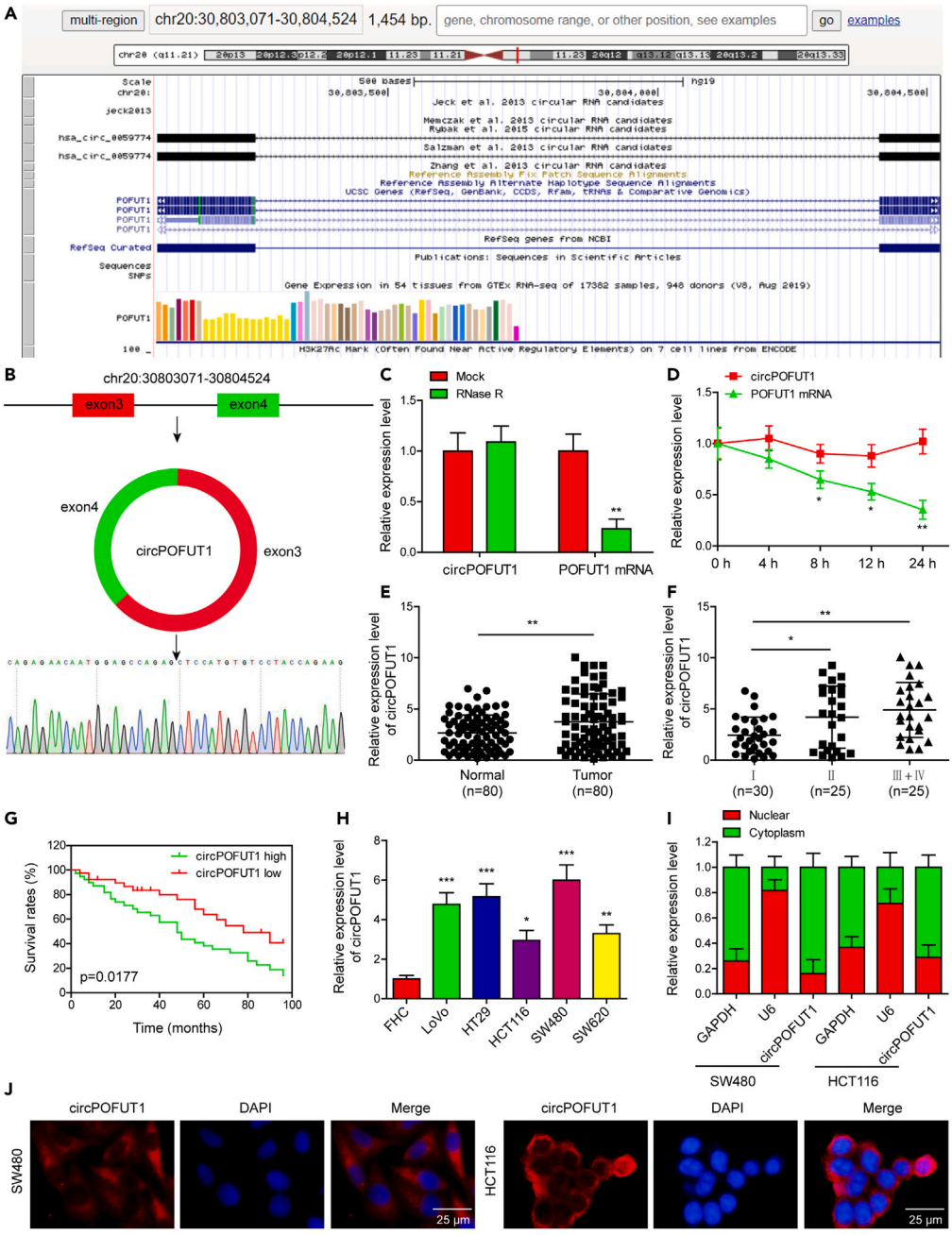

Figure 1. CircPOFUT1 is highly expressed in CRC tissues and cells

(A) Formation of circPOFUT1 based on UCSC.

(B) Schematic drawing and Sanger sequencing illustrated the formation of circPOFUT1.

(C and D) qRT-PCR analysis of circPOFUT1 and POFUT1 mRNA after RNase R or actinomycin D treatment.

(E and F) The circPOFUT1 expression levels in normal and CRC tissues were detected by qRT-PCR.

(G) The correlation between circPOFUT1 expression level and overall survival of patients with CRC was analyzed by Kaplan-Meier method. High and low expression levels of circPOFUT1 were defined based on the median.

(H) The expression levels of circPOFUT1 in CRC cells were detected by qRT-PCR.

(I) qRT-PCR analysis of circPOFUT1 in nuclear and cytoplasmic fractions.

(J) The subcellular localization of circPOFUT1 was detected by RNA FISH. Red, circPOFUT1; Blue, DAPI.

Data are represented as mean ± standard deviation (SD). *$p < 0.05$, **$p < 0.01$, ***$p < 0.001$.

Table 1. Clinicopathological characteristics of patients with colorectal cancer

Characteristics	Cases (n)
Age (years)	
<60 years	34
≥60 years	46
Sex	
Male	49
Female	31
Tumor size (cm)	
<1.5	44
≥1.5	36
TNM stage	
I-II	55
III-IV	25
Histological type	
Adenocarcinoma	48
Mucinous adenocarcinoma	32
Liver metastasis	
Yes	27
No	53

successfully pulled down circPOFUT1 in both SW480 and HCT116 cells (Figure 5D). Also, the binding sites of circPOFUT1 and miR-653-5p were shown (Figure 5E). Additionally, co-localization of circPOFUT1 and miR-653-5p was detected by RNA FISH in both cells (Figure 5F). More important, miR-653-5p was remarkably downregulated in stage II and stage III+IV CRC tissues, compared with stage I CRC tissues, indicating that miR-653-5p level was negatively correlated with TNM stage (Figure 5G). Pearson correlation analysis showed that there was a negative correlation between circPOFUT1 and miR-653-5p in CRC tissues (Figure 5H). In SW480 and HCT116 cells, circPOFUT1 negatively regulated miR-653-5p expression as detected by qRT-PCR (Figure 5I). Collectively, these data suggest that circPOFUT1 serves as a miR-653-5p sponge in CRC cells.

CircPOFUT1 enhances cell proliferation, migration and invasion via modulating miR-653-5p

Functional experiments were next conducted to test whether miR-653-5p was implicated in circPOFUT1-mediated malignant phenotypes of CRC cells. As presented in Figure 6A, sh-circPOFUT1-inhibited colony formation abilities of SW480 cells were rescued by miR-653-5p inhibitor. On the contrary, OE-circPOFUT1-induced colony formation was abrogated by miR-653-5p mimics in HCT116 cells. Similar results were found by Transwell migration and invasion assays (Figure 6B). In addition, sh-circPOFUT1-induced changes of EMT markers were reversed by miR-653-5p inhibitor, whereas the effects of OE-circPOFUT1 on the expression of EMT markers were counteracted by miR-653-5p mimics (Figure 6C). These findings indicate that miR-653-5p plays an indispensable role in circPOFUT1-mediated CRC growth and metastasis.

CircPOFUT1 acts as a competing endogenous RNA and competes with E2F7 to bind miR-653-5p

The binding site of miR-653-5p in 3′UTR of E2F7 was predicted by bioinformatics analysis (Figure 7A). Dual luciferase reporter assay further showed that miR-653-5p mimics markedly decreased the luciferase activity of a construct carrying the wild-type 3′UTR of E2F7 (E2F7 WT), compared with mimics control. By contrast, the mutant of E2F7 (E2F7 MUT) abrogated this effect (Figure 7B). qRT-PCR further revealed that E2F7 was negatively regulated by miR-653-5p (Figure 7C). In addition, circPOFUT1, E2F7 and miR-653-5p were enriched by the antibody against Ago2 as detected by RIP assays in both SW480 and HCT116 cells (Figure 7D), indicating that circPOFUT1 and E2F7 were recruited to Ago2-related RNA-inducing silencing complex (RISC) where they interacted with miR-653-5p. Silencing of circPOFUT1 decreased the enrichment of circPOFUT1 by anti-Ago2 antibody, along with the increased enrichment of E2F7 (Figure 7E), suggesting that circPOFUT1 acted as a ceRNA and competed with E2F7 to bind miRNAs. Additionally, qRT-PCR showed that E2F7 was highly expressed in stage II and stage III+IV CRC tissues, in comparison with stage I CRC tissues (Figure 7F). Together, these data suggest that circPOFUT1 acts as a ceRNA and competes with E2F7 to bind miR-653-5p.

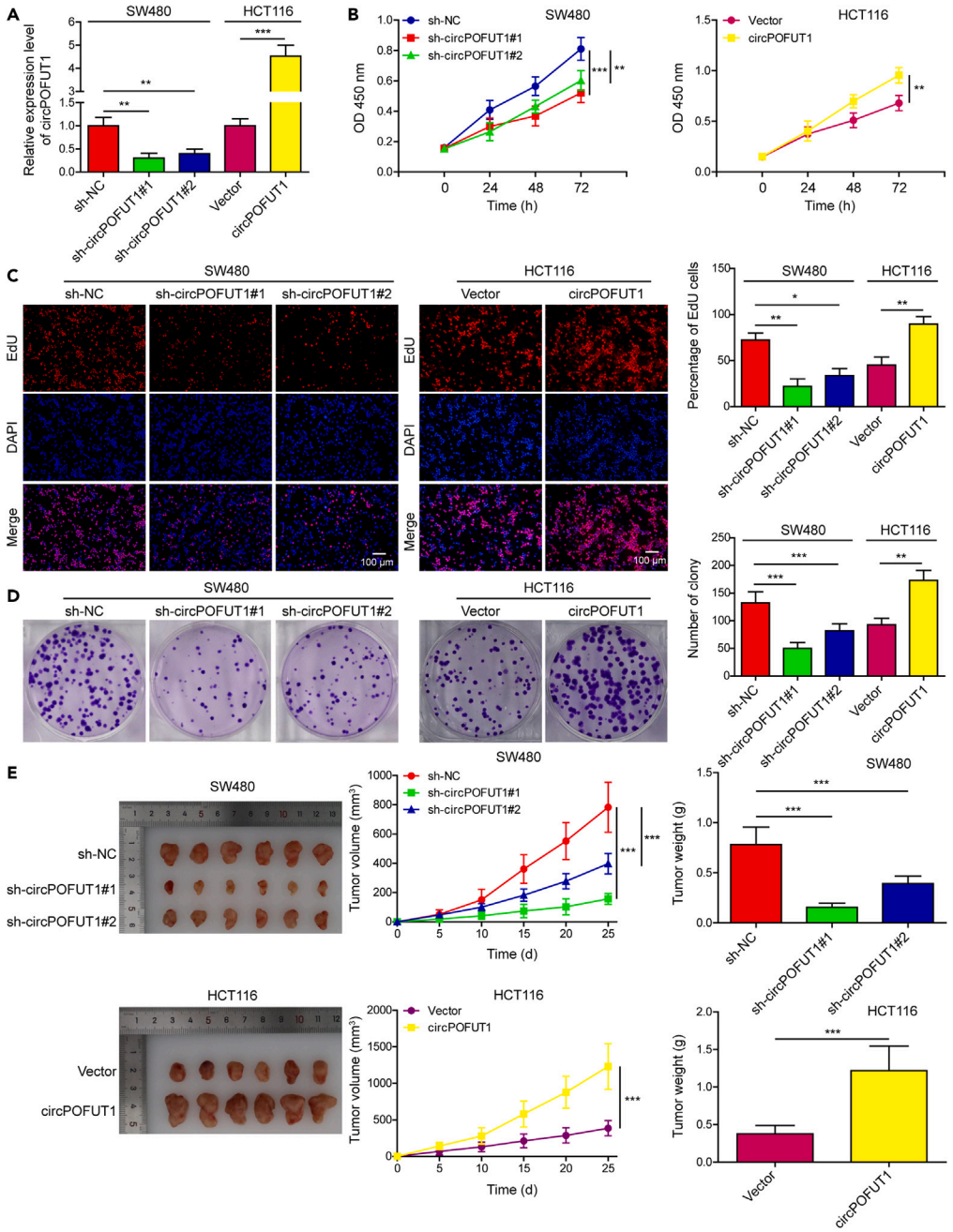

Figure 2. CircPOFUT1 enhances cell proliferation in CRC cells

(A–D) (A) The circPOFUT1 expression levels in circPOFUT1-knockdown or -overexpressing cells were detected by qRT-PCR. Cell proliferation was monitored by (B) CCK-8 assay, (C) EdU incorporation assay and (D) colony formation assay.

(E) Photographs of xenograft tumor with quantitative analysis of tumor volume and weight.

Data are represented as mean ± SD. *p < 0.05, **p < 0.01, ***p < 0.001.

E2F7 is a transcriptional activator of WDR66

Bioinformatics analysis based on UCSC and JASPAR databases predicted that WDR66 promoter region (869–882) contained E2F7 binding sites (Figures 8A and 8B). ChIP assay revealed that anti-E2F7 antibody significantly enriched WDR66, compared with normal IgG control (Figure 8C). Moreover, silencing of E2F7 led to a dramatic reduction of luciferase activity in WDR66 in SW480 cells, whereas overexpression of E2F7 resulted in a marked induction of luciferase activity in WDR66 in HCT116 cells (Figure 8D). Furthermore, significant elevation of WDR66 was observed in CRC cells, and its expression was positively correlated with TNM stage of patients (Figures 8E and 8F). Pearson

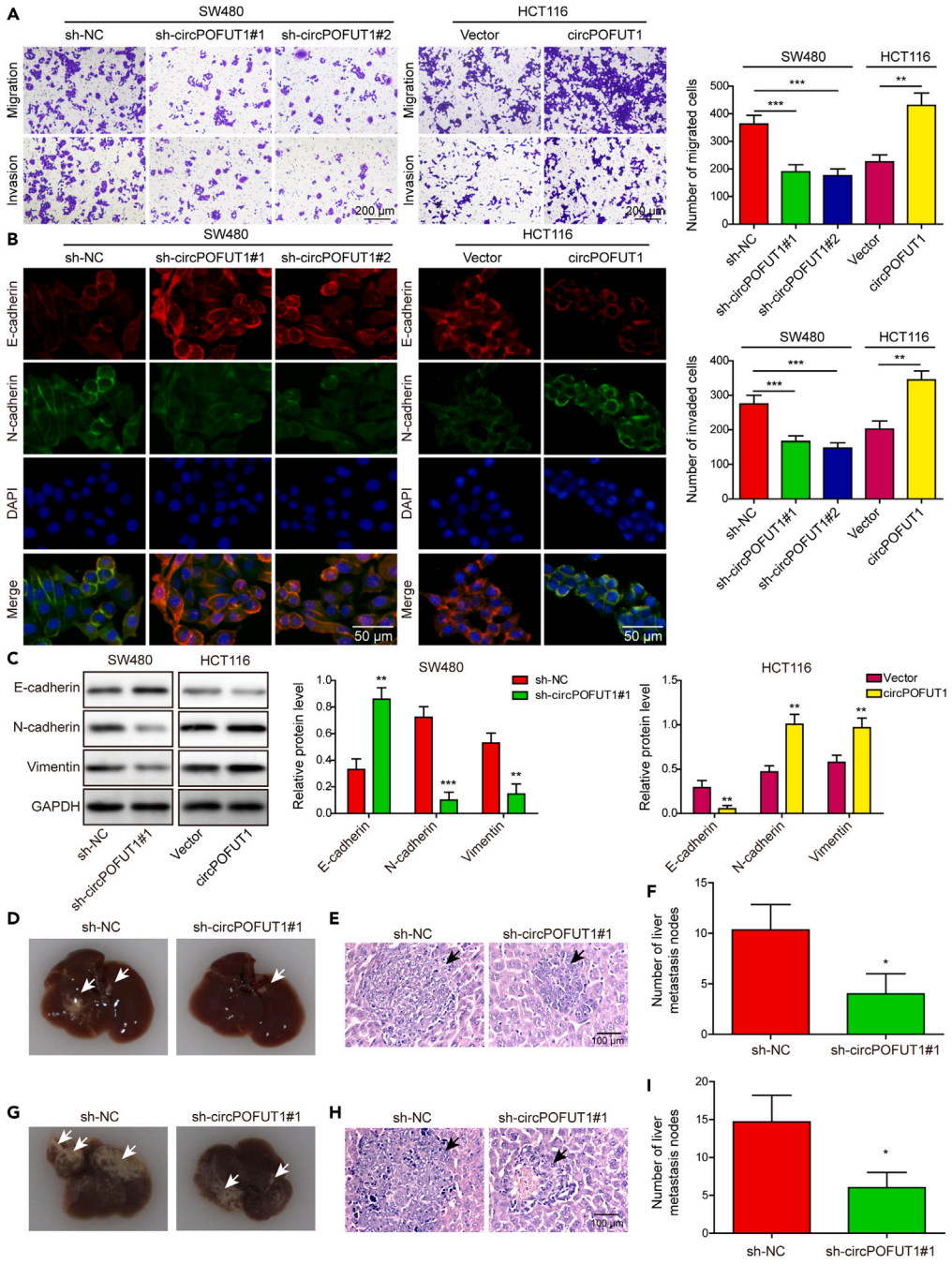

Figure 3. CircPOFUT1 enhances migration and invasion *in vitro* and induces liver metastasis *in vivo*

(A) Cell migration and invasion were detected by Transwell migration and invasion assays.

(B) The expression of E-cadherin and N-cadherin were detected by immunofluorescence.

(C) The expression of E-cadherin, N-cadherin and vimentin were detected by Western blot.

(D) Representative photographs of metastatic nodules in liver tissues via tail-vein injection.

(E and F) H&E staining of liver tissues with quantitative analysis in D.

(G) Representative photographs of metastatic nodules in liver tissues via intra-splenic injection.

(H and I) H&E staining of liver tissues with quantitative analysis in G.

Data are represented as mean ± SD. *$p < 0.05$, **$p < 0.01$, ***$p < 0.001$.

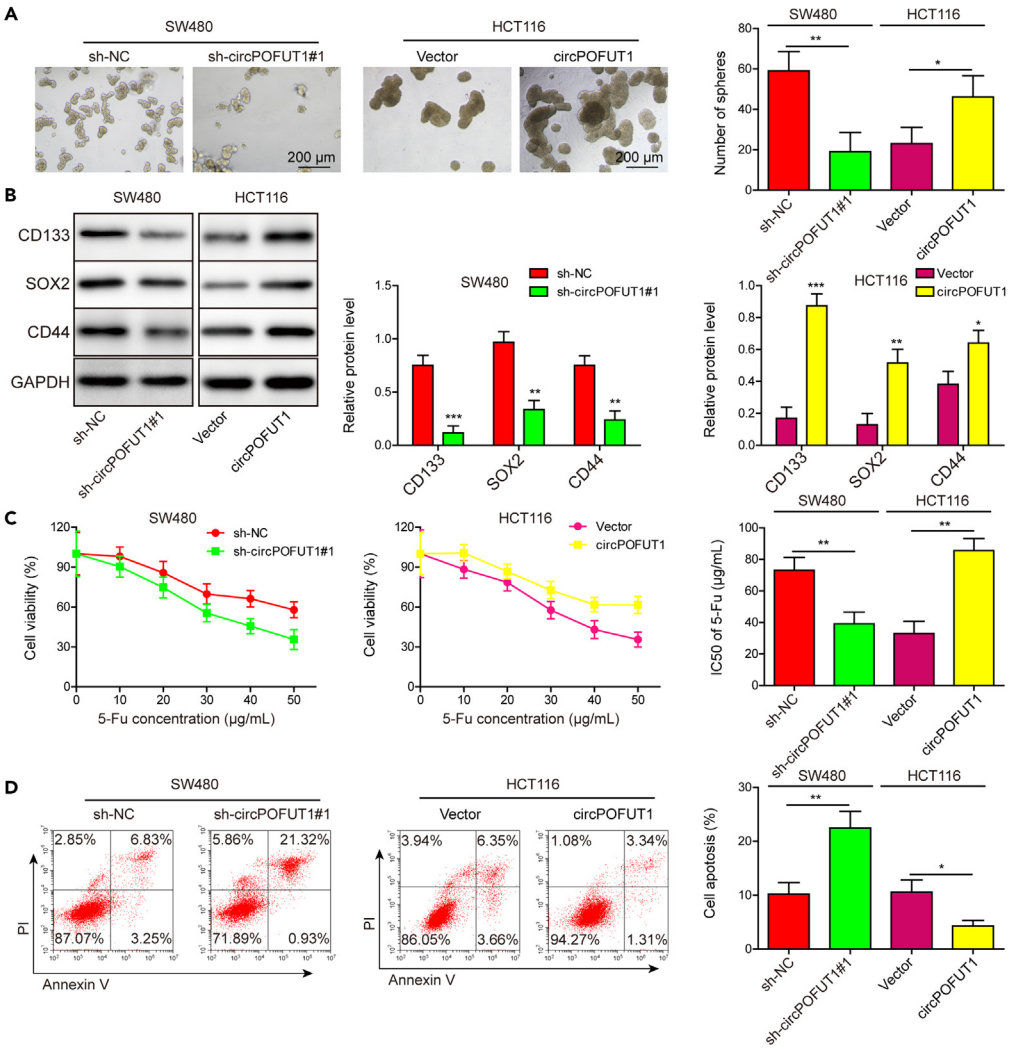

Figure 4. CircPOFUT1 reinforces stem cell-like properties and chemoresistance of CRC cells

(A) Representative sphere images of CRC cells with quantitative analysis.

(B) The expression levels of CD133, SOX2 and CD44 were detected by Western blot.

(C) Cell viability was monitored by CCK-8 assay.

(D) Cell apoptosis was detected by Annexin-V-FITC/PI staining followed by flow cytometry.

Data are represented as mean ± SD. *p < 0.05, **p < 0.01, ***p < 0.001.

correlation analysis revealed a positive correlation between circPOFUT1 and E2F7, as well as between circPOFUT1 and WDR66 in CRC tissues (Figures 8G and 8H). Intriguingly, circPOFUT1 positively regulated WDR66 expression in CRC cells (Figures 8I and 8J). As expected, miR-653-5p inhibitor reversed the decreased E2F7 and WDR66 expression induced by sh-circPOFUT1 in SW480 cells, and miR-653-5p mimics counteracted circPOFUT1-induced increases on these two proteins in HCT116 cells (Figure 8K). Taken together, these findings suggest that E2F7 is a transcriptional activator of WDR66.

WDR66 is implicated in the regulation of colorectal cancer metastasis

As shown in Figure 9A, transwell assays revealed that silencing of WDR66 impaired the migration and invasion of SW480 cells, and co-transfection of sh-WDR66 and circPOFUT1 counteracted these effects. The opposite tendency was observed in HCT116 cells (Figure 9A). Consistently, Western blot and immunofluorescence unequivocally showed that sh-WDR66-or WDR66-mediated changes of EMT markers were reversed by circPOFUT1 overexpression or knockdown in CRC cells, respectively (Figures 9B and 9C), indicating that WDR66 is involved in circPOFUT1-regulated CRC metastasis.

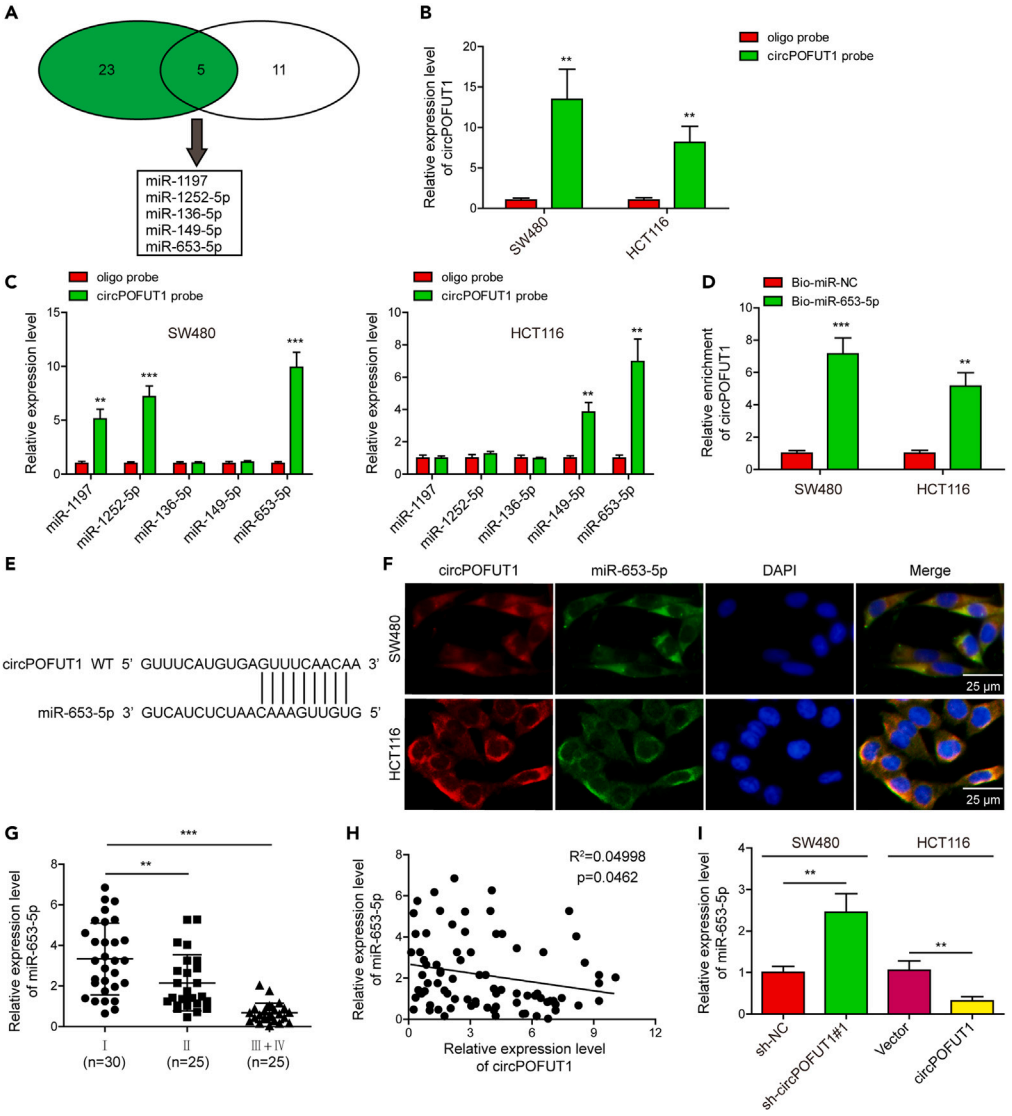

Figure 5. CircPOFUT1 serves as a sponge of miR-653-5p

(A) Bioinformatics analysis of putative circPOFUT1-miRNA interactions.

(B) The specificity of circPOFUT1 probe was verified by RNA pull-down assay.

(C) The interaction between circPOFUT1 and putative miRNAs was verified by RNA pull-down assay.

(D) The interaction between miR-653-5p and circPOFUT1 was verified by RNA pull-down assay.

(E) The binding sites of circPOFUT1 and miR-653-5p.

(F) The subcellular localization of circPOFUT1 and miR-653-5p was detected by RNA FISH. Red, circPOFUT1; Green, miR-653-5p; Blue, DAPI.

(G) The miR-653-5p expression levels in CRC tissues were detected by qRT-PCR.

(H) The correlation between circPOFUT1 and miR-653-5p in CRC tissues was analyzed by Pearson correlation analysis.

(I) The miR-653-5p expression levels in CRC cells were detected by qRT-PCR.

Data are represented as mean ± SD. **p < 0.01, ***p < 0.001.

CircPOFUT1 stabilizes B-cell-specific moloney leukemia virus insertion site 1 mRNA via recruiting insulin-like growth factor 2 mRNA-binding protein 1

We next delineated the underlying mechanism by which circPOFUT1 regulated stemness and chemoresistance in CRC. Interestingly, RNA pull-down assay showed that circPOFUT1 interacted with the stemness marker B-cell-specific moloney leukemia virus insertion site 1 (BMI1) in both SW480 and HCT116 cells (Figure 10A). Additionally, qRT-PCR revealed that BMI1 was positively regulated by circPOFUT1 (Figure 10B), and circPOFUT1 enhanced the mRNA stability of BMI1 in both SW480 and HCT116 cells (Figure 10C). Furthermore, the elevation of BMI1 was also observed in stage II and stage III+IV CRC tissues, compared with stage I CRC tissues, suggesting that its expression was

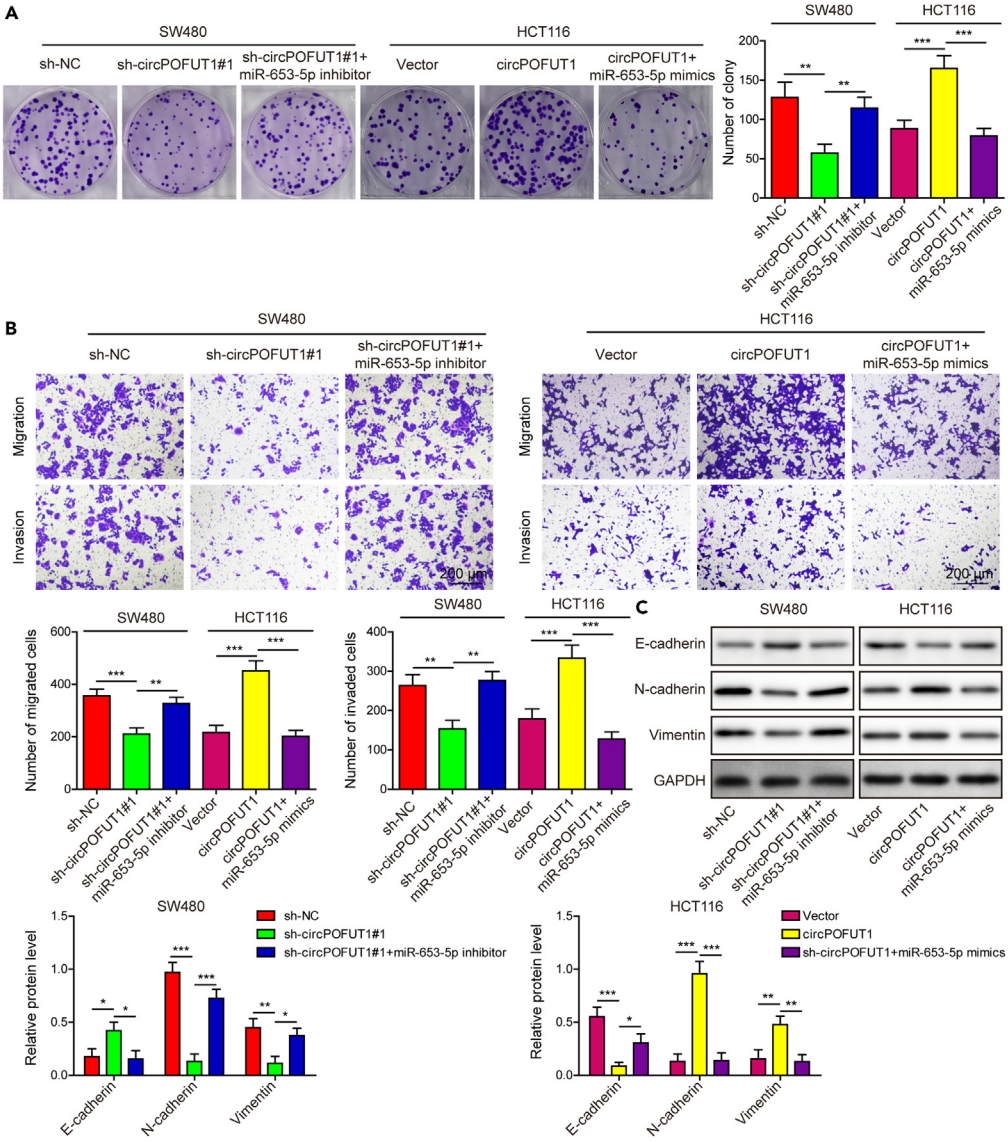

Figure 6. CircPOFUT1 enhances cell proliferation, migration and invasion via modulating miR-653-5p

(A) Cell proliferation was monitored by colony formation assay.

(B) Cell migration and invasion were detected by Transwell migration and invasion assays.

(C) The expression levels of E-cadherin, N-cadherin and vimentin were detected by Western blot.

Data are represented as mean ± SD. *p < 0.05, **p < 0.01, ***p < 0.001.

positively correlated with TNM stage (Figure 10D). Pearson correlation analysis showed that there was a positive correlation between circPOFUT1 and BMI1 expression in CRC tissues (Figure 10E). Our preliminary bioinformatics analysis predicted that circPOFUT1 might directly associate with insulin-like growth factor 2 mRNA-binding protein 1 (IGF2BP1). Moreover, recent study has illustrated that lncRNA NEAT1 enhanced the interaction between IGF2BP1 and ELF3 mRNA, thereby stabilizing ELF3 mRNA in pancreatic cancer,[18] raising the possibility that circPOFUT1 might stabilize BMI1 mRNA via recruiting IGF2BP1 in CRC cells. To test this hypothesis, RIP assay was conducted. As presented in Figures 10F and 10G, anti-IGF2BP1 successfully enriched circPOFUT1 in CRC cells. Moreover, qRT-PCR further showed that IGF2BP1 positively regulated BMI1 expression in both SW480 and HCT116 cells (Figures 10H and 10I). Overexpression of circPOFUT1 led to a remarkable induction of BMI1, and this effect was attenuated by IGF2BP1 knockdown (Figure 10J), indicating that IGF2BP1 acted as a key player in circPOFUT1-mediated regulation of BMI1 in CRC cells. Collectively, these findings indicate that circPOFUT1 stabilizes BMI1 mRNA via recruiting IGF2BP1.

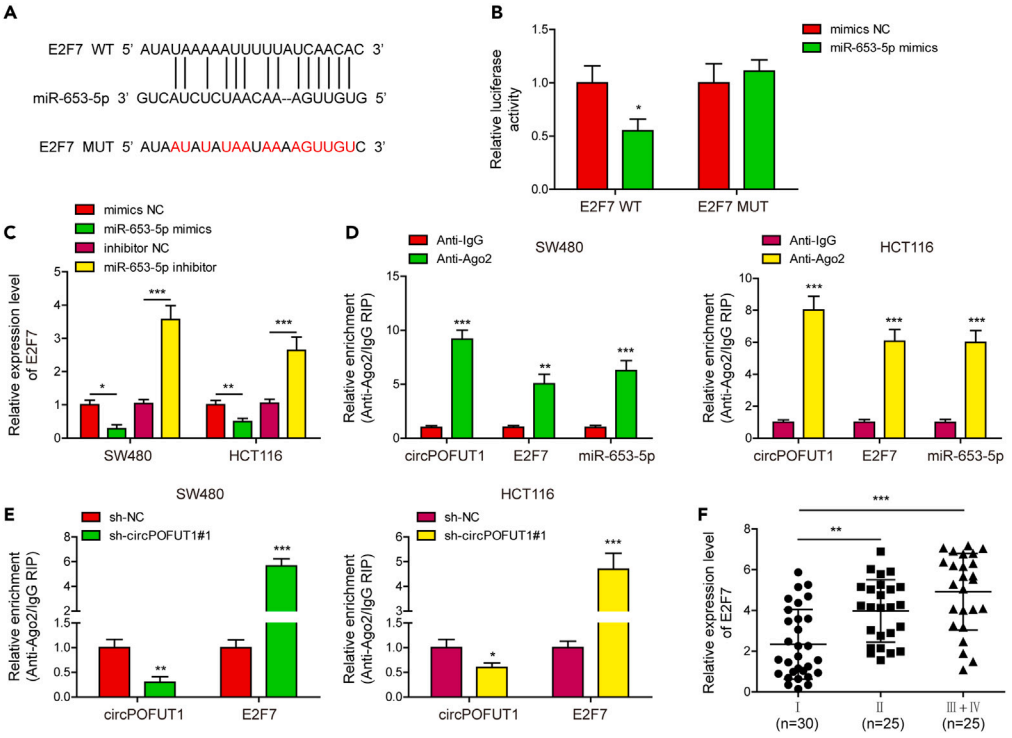

Figure 7. CircPOFUT1 acts as a ceRNA and competes with E2F7 to bind miR-653-5p

(A) Putative binding site between miR-653-5p and E2F7 3′UTR was predicted by bioinformatics analysis.

(B) Relative luciferase activity was detected by dual luciferase reporter assay.

(C) The mRNA levels of E2F7 in CRC cells were determined by qRT-PCR.

(D and E) The interactions among circPOFUT1, E2F7 and miR-653-5p were detected by RIP assay.

(F) The mRNA levels of E2F7 in CRC tissues were detected by qRT-PCR.

Data are represented as mean ± SD. *p < 0.05, **p < 0.01, ***p < 0.001.

CircPOFUT1 promotes stemness and chemoresistance of colorectal cancer cells partially via stabilizing B-cell-specific moloney leukemia virus insertion site 1

Functional experiments were then carried out to investigate the roles of circPOFUT1/BMI1 axis in CRC cells. As shown in Figure 11A, sh-circPOFUT1-suppressed sphere forming the ability of SW480 cells was rescued by BMI overexpression, while circPOFUT1-enhanced sphere forming the ability of HCT116 cells was abrogated by BMI1 silencing. In addition, the effects of sh-circPOFUT1 or OE-circPOFUT1 on the expression of CD133, SOX2 and CD44 in CRC cells were reversed by BMI overexpression or knockdown, respectively (Figure 11B). CCK-8 assay and Annexin-V/PI staining were further performed to monitor the effects of circPOFUT1/BMI1 axis on chemoresistance in CRC cells. As presented in Figure 11C, silencing of circPOFUT1 enhanced the sensitivity of SW480 cells to 5-Fu, while the effect was counteracted by BMI1 overexpression. In HCT116 cells, OE-circPOFUT1-increased chemoresistance to 5-Fu was attenuated by BMI1 silencing (Figure 11C). In accordance with these results, sh-circPOFUT1-increased apoptosis was reversed by BMI1 overexpression in SW480 cells, while OE-circPOFUT1-suppressed apoptosis was reversed by BMI1 knockdown (Figure 11D). Taken together, these data indicate that circPOFUT1 promotes stemness and chemoresistance of CRC cells partially via stabilizing BMI1.

DISCUSSION

Increasing incidence of CRC has been found in young and middle-aged adults in recent years, and this may be attributed to increased sedentary behavior, westernized diet and obesity.[1,16] Metastasis, chemoresistance and recurrence remain the key challenges for CRC treatment.[2] The rising incidence and poor prognosis of CRC highlight the urgent need to identify biomarkers and gain an in-depth understanding of underlying mechanism. In the present study, we reported that circPOFUT1 expression was elevated in CRC tissues and cells, and it exerted an oncogenic role in CRC. Mechanistic investigation revealed that circPOFUT1 enhanced metastasis via regulating miR-653-5p/E2F7/WDR66 axis, and it promoted stemness and chemoresistance through stabilizing BMI1 mRNA in a IGF2BP1-dependent manner.

CircRNAs have gained wide attention for their involvement in cancers as diagnostic or therapeutic biomarkers.[19] In the current study, one circRNA, namely hsa_circ_0059774, was identified. It formed via circularization of POFUT1 pre-mRNA, thus it was designated as circPOFTU1.

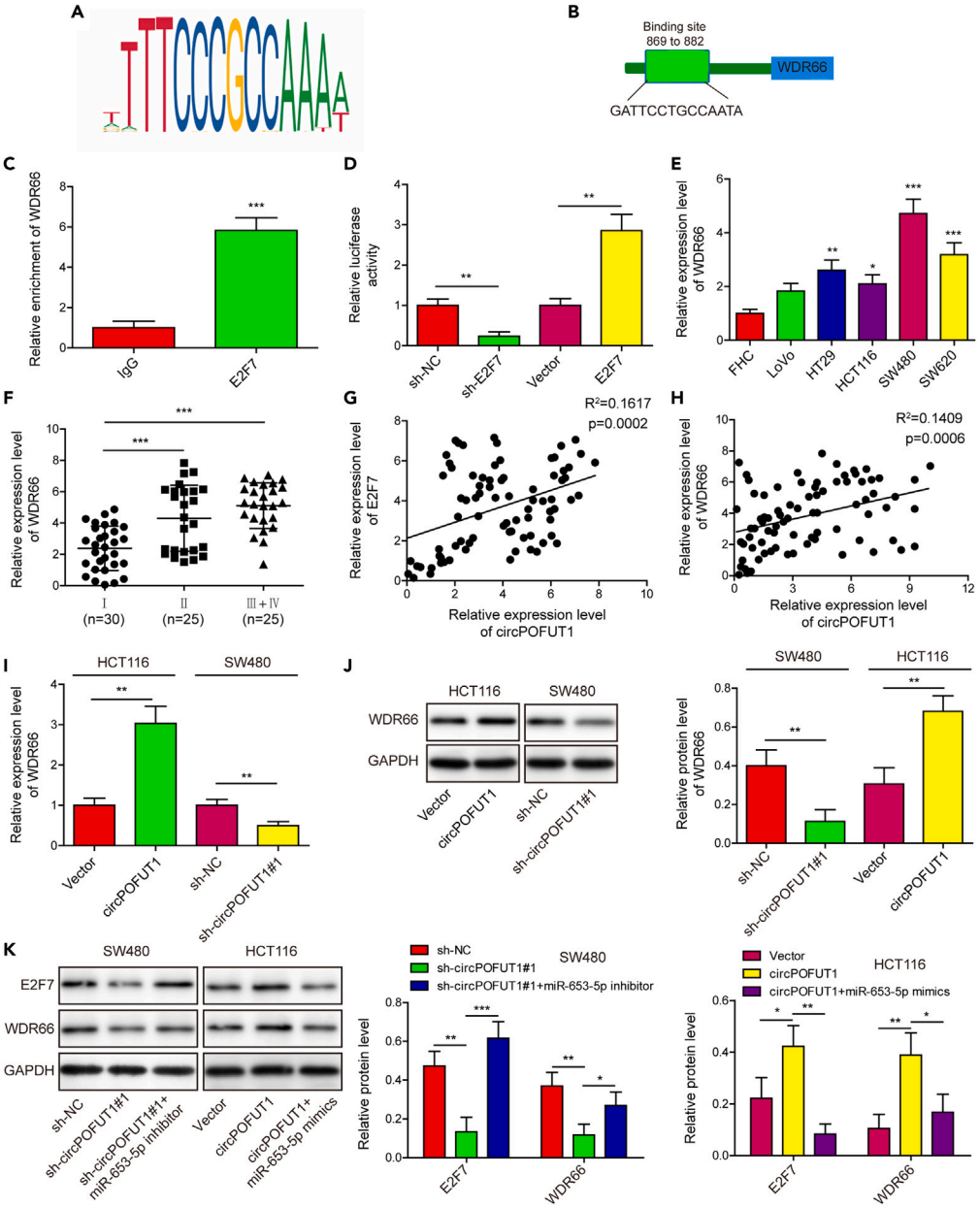

Figure 8. E2F7 is a transcriptional activator of WDR66

(A and B) Bioinformatics analysis about the binding sites between E2F7 and WDR66 promoter region using UCSC and JASPAR databases.

(C) The direct interaction between E2F7 and WDR66 promoter was detected by ChIP assay.

(D) The direct interaction between E2F7 and WDR66 promoter was detected by luciferase reporter assay.

(E) The mRNA levels of WDR66 in different CRC cells were determined by qRT-PCR.

(F) The mRNA levels of WDR66 in CRC tissues were detected by qRT-PCR.

(G) The correlation between circPOFUT1 and E2F7 in CRC tissues was analyzed by Pearson correlation analysis.

(H) The correlation between circPOFUT1 and WDR66 in CRC tissues was analyzed by Pearson correlation analysis.

(I) The mRNA levels of WDR66 in transfected HCT116 and SW480 cells were detected by qRT-PCR. (J) The protein levels of WDR66 in CRC cells were detected by Western blot.

(K) The protein levels of E2F7 and WDR66 in CRC cells were detected by Western blot.

Data are represented as mean ± SD. *p < 0.05, **p < 0.01, ***p < 0.001.

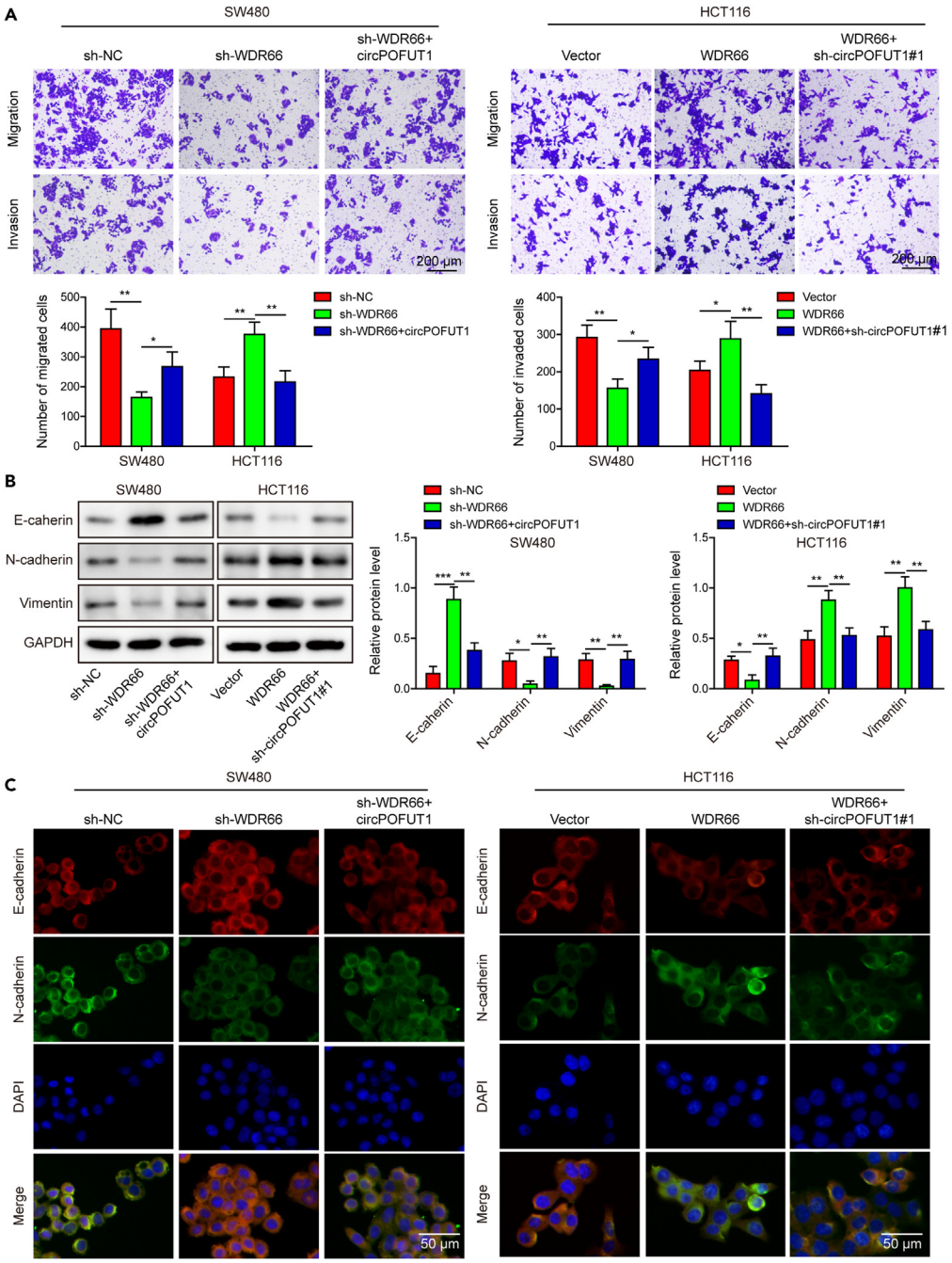

Figure 9. WDR66 is implicated in the regulation of CRC metastasis

(A) Cell migration and invasion were detected by Transwell migration and invasion assays.

(B) The expression levels of E-cadherin, N-cadherin and vimentin were detected by Western blot.

(C) The expression of E-cadherin and N-cadherin were detected by immunofluorescence.

Data are represented as mean ± SD. *p < 0.05, **p < 0.01, ***p < 0.001.

Previous studies have demonstrated that POFUT1 promotes CRC progression via Notch1 signaling.[17,20,21] POFUT1 and PLAGL2 share a bidirectional promoter, and work in concert to promote CRC progression.[22] Our preliminary data illustrated the upregulation of circPOFUT1 in CRC tissues and cells, raising the possibility that circPOFUT1 might be a key player in CRC progression. Functional experiments further showed that circPOFUT1 promoted cell proliferation, migration, invasion and EMT *in vitro*, and it also promoted tumor growth and liver metastasis *in vivo*. We have demonstrated that circPOFUT1 acted as an oncogene in CRC.

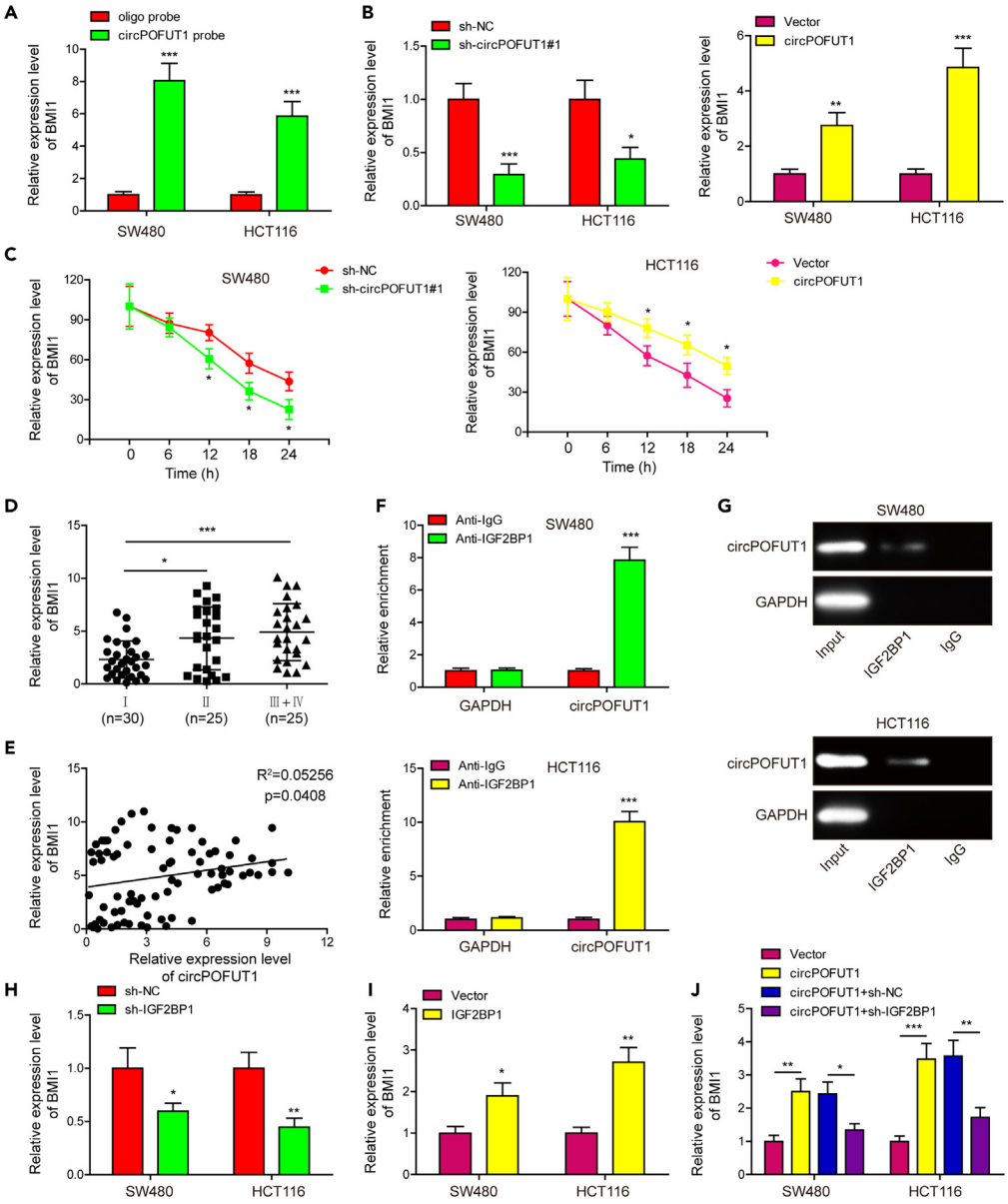

Figure 10. CircPOFUT1 stabilizes BMI1 mRNA via recruiting IGF2BP1

(A) The interaction between circPOFUT1 and BMI1 mRNA was detected by RNA pull-down assay.

(B) The mRNA levels of BMI1 in CRC cells were determined by qRT-PCR.

(C) The mRNA stability of BMI1 was detected by qRT-PCR.

(D) The BMI1 expression levels in CRC tissues were detected by qRT-PCR.

(E) The correlation between circPOFUT1 and BMI1 in CRC tissues was analyzed by Pearson correlation analysis.

(F and G) The interaction between circPOFUT1 and IGF2BP1 was detected by RIP assay.

(H–J) The mRNA levels of BMI1 in CRC cells were determined by qRT-PCR.

Data are represented as mean ± SD. *p < 0.05, **p < 0.01, ***p < 0.001.

The competing endogenous RNA (ceRNA) hypothesis suggests that circRNA competes with mRNA to bind miRNA via one or multiple miRNA response elements.[23] CircRNAs thus induce the expression of target genes by sponging miRNAs. A number of circRNA-miRNA-mRNA networks have been reported in CRC.[16] For instance, hsa_circ_001680 contributed to cell proliferation, migration and chemoresistance of CRC by modulating miR-340/BMI1 axis.[24] Bioinformatics analysis and validation experiments revealed that circPOFUT1 acted as a sponge of miR-653-5p. MiR-653-5p exerted either oncogenic or tumor suppressive effects in different cancers. Previous studies reported that miR-653-5p promoted gastric cancer progression via SOCS6/STAT3 pathway, while it inhibited breast cancer growth and metastasis by targeting MAPK6.[25,26] We

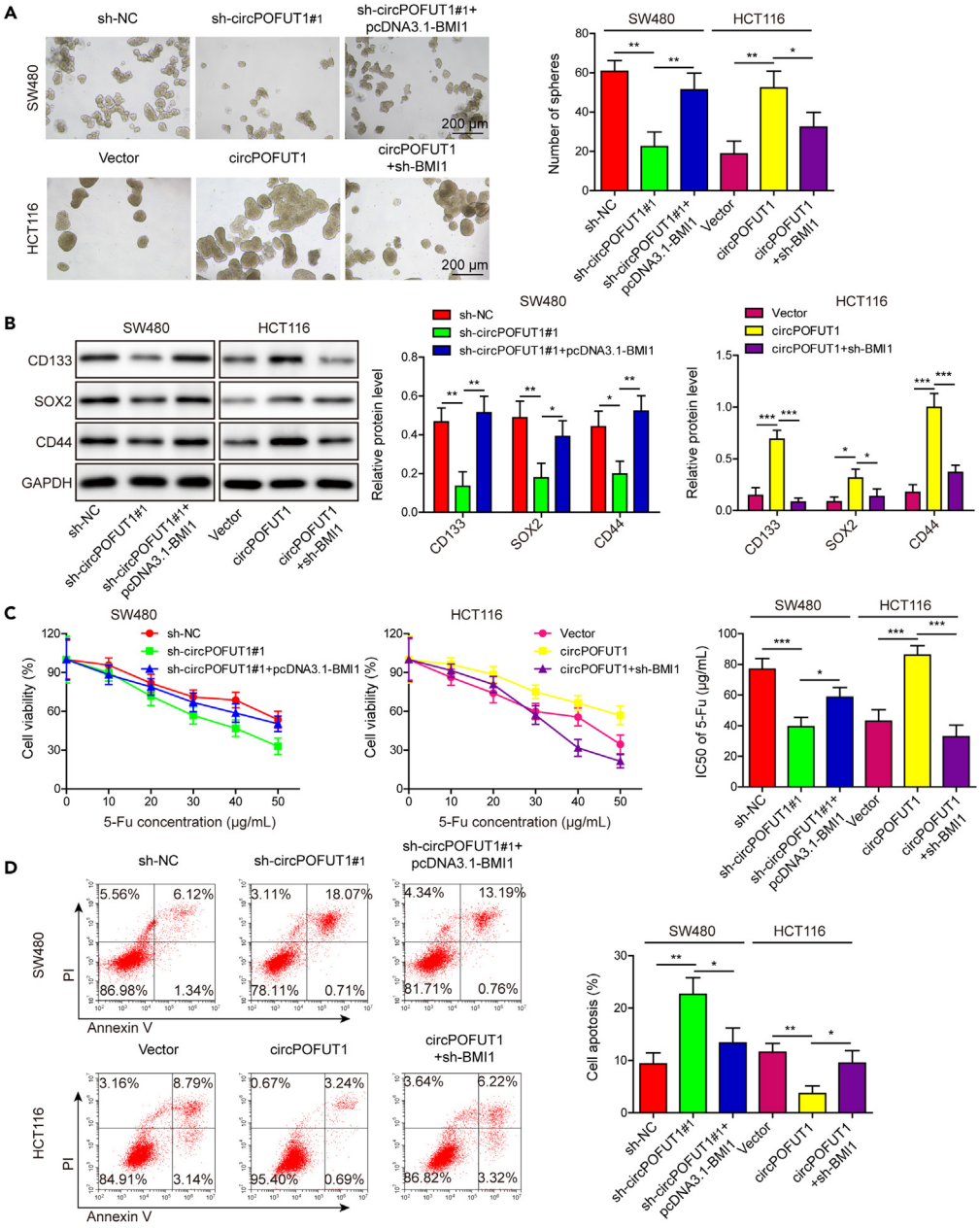

Figure 11. CircPOFUT1 promotes stemness and chemoresistance of CRC cells partially via stabilizing BMI1

(A) Representative sphere images of CRC cells with quantitative analysis.

(B) The expression of CD133, SOX2 and CD44 were detected by Western blot.

(C) Cell viability was monitored by CCK-8 assay.

(D) Cell apoptosis was detected by Annexin-V-FITC/PI staining followed by flow cytometry.

Data are represented as mean ± SD. *p < 0.05, **p < 0.01, ***p < 0.001.

demonstrated that miR-653-5p was downregulated in CRC tissues. Although the gain- and loss-of function experiments revealed that WDR66 might be a downstream effector of circPOFUT1-induced CRC metastasis, no direct interaction was identified between miR-653-5p and WDR66. Interestingly, bioinformatics analysis predicted E2F7 binding site in WDR66 promoter region, as well as the miR-653-5p binding site in 3′UTR of E2F7. Subsequent experiments further supported that circPOFUT1 regulated E2F7 via sequestering miR-653-5p, thereby inducing WDR66 expression in CRC cells. In addition, lack of WDR66 impaired the migration and invasion in CRC cells. WDR66 is highly expressed in esophageal squamous cell carcinoma (ESCC), and contributes to ESCC growth and metastasis as a positive modulator of EMT.[27] In line with this report, our findings showed that WDR66 served as a key effector in circPOFUT1-mediated CRC growth and metastasis. Furthermore, E2F7, a transcriptional

activator of WDR66, is well-accepted as a downstream molecule of p53 and contributes to DNA damage-induced cell-cycle arrest.[28] The regulatory relationship between p53 and circPOFUT1/miR-653-5p/E2F7/WDR66 axis in CRC needs further investigation.

Besides acting as ceRNAs, circRNAs also exerted the biological roles via interacting with RNA binding proteins (RBPs).[29] For instance, it has been reported that circFOXO3 forms ternary complexes with p21 and CDK2 to arrest cell cycle progression.[30] IGF2BP1 is a conserved RBP which has been revealed to participate in lncRNA-mediated mRNA stabilization.[18] In addition to this report, our findings further illustrated that IGF2BP1 was implicated in circPOFUT1-mediated BMI1 mRNA stabilization. BMI1 is upregulated in CRC and acts as a crucial regulator of CSC self-renewal and plasticity.[31,32] Consistently, our data showed that BMI1 was significantly elevated in CRC tissues, and there was a positive correlation between circPOFUT1 and BMI1 in CRC. Functional experiments further confirmed that BMI1 was an important effector in circPOFUT1-regulated stemness and chemoresistance. Two regulatory axes have been reported in this study, however, it is unclear whether there is a crosstalk between the two.

In conclusion, we demonstrate that circPOFUT1 promotes CRC metastasis via decoying miR-653-5p/E2F7/WDR66 axis, and contributes to chemoresistance via stabilizing BMI1 mRNA in an IGF2BP1-dependent manner.

Limitations of the study

Limitations of the study include the following: Firstly, the metastasis, stemness and chemoresistance effects caused by circPOFUT1/miR-653-5p/E2F7/WDR66 axis or circPOFUT1/IGF2BP1/BMI1 axis need to be validated in the *in vivo* model in the future study. In addition, the upstream mechanism of the circPOFUT1 upregulation in CRC requires further investigation.

STAR★METHODS

Detailed methods are provided in the online version of this paper and include the following:

- KEY RESOURCES TABLE
- RESOURCE AVAILABILLITY
  - Lead contact
  - Materials availability
  - Data and code availability
- EXPERIMENTAL MODEL AND STUDY PARTICIPANT DETAILS
  - Animals
  - Clinical specimens
  - Cells
- METHOD DETAILS
  - Animal study and H&E staining
  - Cell culture and treatment
  - Plasmid construction and transfection
  - Subcellular fractionation
  - RNA Fluorescence *in situ* hybridization (FISH)
  - Cell proliferation assay
  - EdU incorporation assay
  - Colony formation assay
  - Transwell migration and invasion assays
  - Immunofluorescence assay
  - Flow cytometry assay
  - Sphere formation assay
  - qRT-PCR
  - Western blot
  - RNA pull-down assay
  - Dual luciferase reporter assay
  - RNA immunoprecipitation (RIP) assay
  - Chromatin immunoprecipitation (ChIP) assay
- QUANTIFICATION AND STATISTICAL ANALYSIS

SUPPLEMENTAL INFORMATION

Supplemental information can be found online at https://doi.org/10.1016/j.isci.2023.108729.

ACKNOWLEDGMENTS

This work was supported by the National Natural Science Foundation of China (No. 82303255), the Natural Science Foundation of Hunan Province (No. 2023JJ40894, 2023JJ30824, 2021JJ31019) and the Natural Science Foundation of Changsha (No. kq2208361).

AUTHOR CONTRIBUTIONS

F.L. and B.T. designed and performed most of the experiments. L.L., M.M., and Z.C. collected and analyzed the data. G.T. and N.Y. performed bioinformatical analyses. C.Z. and B.Y. performed animal experiments. Y.G. and M.C. interpreted the data. F.L., B.T., and G.H. wrote the article with inputs from all the authors. G.H. designed, supervised, and coordinated the work. All authors read and approved the final article.

DECLARATION OF INTERESTS

The authors declare no competing interests.

Received: April 6, 2023
Revised: October 31, 2023
Accepted: December 11, 2023
Published: December 14, 2023

REFERENCES

1. Siegel, R.L., Miller, K.D., Fuchs, H.E., and Jemal, A. (2021). Cancer Statistics, 2021. CA Cancer J Clin *71*, 7–33.
2. Siegel, R.L., Miller, K.D., Goding Sauer, A., Fedewa, S.A., Butterly, L.F., Anderson, J.C., Cercek, A., Smith, R.A., and Jemal, A. (2020). Colorectal cancer statistics, 2020. CA Cancer J Clin *70*, 145–164.
3. Dienstmann, R., Vermeulen, L., Guinney, J., Kopetz, S., Tejpar, S., and Tabernero, J. (2017). Consensus molecular subtypes and the evolution of precision medicine in colorectal cancer. Nat. Rev. Cancer *17*, 268.
4. Zheng, Y., Zhou, J., and Tong, Y. (2015). Gene signatures of drug resistance predict patient survival in colorectal cancer. Pharmacogenomics J. *15*, 135–143.
5. Brabletz, T., Jung, A., Spaderna, S., Hlubek, F., and Kirchner, T. (2005). Opinion: migrating cancer stem cells - an integrated concept of malignant tumour progression. Nat. Rev. Cancer *5*, 744–749.
6. Clevers, H. (2011). The cancer stem cell: premises, promises and challenges. Nat. Med. *17*, 313–319.
7. Dean, M., Fojo, T., and Bates, S. (2005). Tumour stem cells and drug resistance. Nat. Rev. Cancer *5*, 275–284.
8. Dembinski, J.L., and Krauss, S. (2009). Characterization and functional analysis of a slow cycling stem cell-like subpopulation in pancreas adenocarcinoma. Clin. Exp. Metastasis *26*, 611–623.
9. Singh, A., and Settleman, J. (2010). EMT, cancer stem cells and drug resistance: an emerging axis of evil in the war on cancer. Oncogene *29*, 4741–4751.
10. Jeck, W.R., Sorrentino, J.A., Wang, K., Slevin, M.K., Burd, C.E., Liu, J., Marzluff, W.F., and Sharpless, N.E. (2013). Circular RNAs are abundant, conserved, and associated with ALU repeats. RNA *19*, 141–157.
11. Jeck, W.R., and Sharpless, N.E. (2014). Detecting and characterizing circular RNAs. Nat. Biotechnol. *32*, 453–461.
12. Liu, C.X., Li, X., Nan, F., Jiang, S., Gao, X., Guo, S.K., Xue, W., Cui, Y., Dong, K., Ding, H., et al. (2019). Structure and Degradation of Circular RNAs Regulate PKR Activation in Innate Immunity. Cell *177*, 865–880.e21.
13. Hansen, T.B., Jensen, T.I., Clausen, B.H., Bramsen, J.B., Finsen, B., Damgaard, C.K., and Kjems, J. (2013). Natural RNA circles function as efficient microRNA sponges. Nature *495*, 384–388.
14. Du, W.W., Zhang, C., Yang, W., Yong, T., Awan, F.M., and Yang, B.B. (2017). Identifying and Characterizing circRNA-Protein Interaction. Theranostics *7*, 4183–4191.
15. Pamudurti, N.R., Bartok, O., Jens, M., Ashwal-Fluss, R., Stottmeister, C., Ruhe, L., Hanan, M., Wyler, E., Perez-Hernandez, D., Ramberger, E., et al. (2017). Translation of CircRNAs. Mol. Cell *66*, 9–21.e7.
16. Li, A., Wang, W.C., McAlister, V., Zhou, Q., and Zheng, X. (2021). Circular RNA in colorectal cancer. J. Cell Mol. Med. *25*, 3667–3679.
17. Du, Y., Li, D., Li, N., Su, C., Yang, C., Lin, C., Chen, M., Wu, R., Li, X., and Hu, G. (2018). POFUT1 promotes colorectal cancer development through the activation of Notch1 signaling. Cell Death Dis. *9*, 995.
18. Feng, Y., Gao, L., Cui, G., and Cao, Y. (2020). LncRNA NEAT1 facilitates pancreatic cancer growth and metastasis through stabilizing ELF3 mRNA. Am. J. Cancer Res. *10*, 237–248.
19. Shang, Q., Yang, Z., Jia, R., and Ge, S. (2019). The novel roles of circRNAs in human cancer. Mol. Cancer *18*, 6.
20. Deschuyter, M., Pennarubia, F., Pinault, E., Legardinier, S., and Maftah, A. (2020). Functional Characterization of POFUT1 Variants Associated with Colorectal Cancer. Cancers *12*, 1430.
21. Komor, M.A., de Wit, M., van den Berg, J., Martens de Kemp, S.R., Delis-van Diemen, P.M., Bolijn, A.S., Tijssen, M., Schelfhorst, T., Piersma, S.R., Chiasserini, D., et al. (2020). Molecular characterization of colorectal adenomas reveals POFUT1 as a candidate driver of tumor progression. Int. J. Cancer *146*, 1979–1992.
22. Li, D., Lin, C., Li, N., Du, Y., Yang, C., Bai, Y., Feng, Z., Su, C., Wu, R., Song, S., et al. (2019). PLAGL2 and POFUT1 are regulated by an evolutionarily conserved bidirectional promoter and are collaboratively involved in colorectal cancer by maintaining stemness. EBioMedicine *45*, 124–138.
23. Panda, A.C. (2018). Circular RNAs Act as miRNA Sponges. Adv. Exp. Med. Biol. *1087*, 67–79.
24. Jian, X., He, H., Zhu, J., Zhang, Q., Zheng, Z., Liang, X., Chen, L., Yang, M., Peng, K., Zhang, Z., et al. (2020). Hsa_circ_001680 affects the proliferation and migration of CRC and mediates its chemoresistance by regulating BMI1 through miR-340. Mol. Cancer *19*, 20.
25. Li, Z., Fan, H., Chen, W., Xiao, J., Ma, X., Ni, P., Xu, Z., and Yang, L. (2021). MicroRNA-653-5p Promotes Gastric Cancer Proliferation and Metastasis by Targeting the SOCS6-STAT3 Pathway. Front. Mol. Biosci. *8*, 655580.
26. Zhang, M., Wang, H., Zhang, X., and Liu, F. (2021). miR6535p suppresses the growth and migration of breast cancer cells by targeting MAPK6. Mol. Med. Rep. *23*, 200.
27. Wang, Q., Ma, C., and Kemmner, W. (2013). Wdr66 is a novel marker for risk stratification and involved in epithelial-mesenchymal transition of esophageal squamous cell carcinoma. BMC Cancer *13*, 137.
28. Carvajal, L.A., Hamard, P.J., Tonnessen, C., and Manfredi, J.J. (2012). E2F7, a novel target, is up-regulated by p53 and mediates DNA damage-dependent transcriptional repression. Genes Dev. *26*, 1533–1545.
29. Huang, A., Zheng, H., Wu, Z., Chen, M., and Huang, Y. (2020). Circular RNA-protein interactions: functions, mechanisms, and identification. Theranostics *10*, 3503–3517.
30. Du, W.W., Yang, W., Liu, E., Yang, Z., Dhaliwal, P., and Yang, B.B. (2016). Foxo3 circular RNA retards cell cycle progression via forming ternary complexes with p21 and CDK2. Nucleic Acids Res. *44*, 2846–2858.
31. Pun, J.C.S., Chan, J.Y.J., Chun, B.K.M., Ng, K.W., Tsui, S.Y.K., Wan, T.M.H., Lo, O., Poon, J.T.C., Ng, L., and Pang, R. (2014). Plasma Bmi1 mRNA as a potential prognostic biomarker for distant metastasis in colorectal cancer patients. Mol. Clin. Oncol. *2*, 817–820.
32. Alajez, N.M. (2016). Significance of BMI1 and FSCN1 expression in colorectal cancer. Saudi J. Gastroenterol. *22*, 288–293.
33. Nie, S., Zhou, J., Bai, F., Jiang, B., Chen, J., and Zhou, J. (2014). Role of endothelin A receptor in colon cancer metastasis: in vitro and in vivo evidence. Mol. Carcinog. *53*, E85–E91.

34. Xu, Y., Zhang, L., Wang, Q., and Zheng, M. (2020). Comparison of Different Colorectal Cancer With Liver Metastases Models Using Six Colorectal Cancer Cell Lines. Pathol. Oncol. Res. *26*, 2177–2183.

35. Konstantopoulos, P., Doulamis, I.P., Tzani, A., Korou, M.L., Agapitos, E., Vlachos, I.S., Pergialiotis, V., Verikokos, C., Mastorakos, G., Katsilambros, N.L., and Perrea, D.N. (2017). Metabolic effects of Crocus sativus and protective action against non-alcoholic fatty liver disease in diabetic rats. Biomed. Rep. *6*, 513–518.

36. Yang, X., Liu, L., Zou, H., Zheng, Y.W., and Wang, K.P. (2019). circZFR promotes cell proliferation and migration by regulating miR-511/AKT1 axis in hepatocellular carcinoma. Dig. Liver Dis. *51*, 1446–1455.

37. Bai, Y., Yang, C., Wu, R., Huang, L., Song, S., Li, W., Yan, P., Lin, C., Li, D., and Zhang, Y. (2019). YTHDF1 Regulates Tumorigenicity and Cancer Stem Cell-Like Activity in Human Colorectal Carcinoma. Front. Oncol. *9*, 332.

STAR★METHODS

KEY RESOURCES TABLE

REAGENT or RESOURCE	SOURCE	IDENTIFIER
Antibodies		
E-cadherin	Abcam	Cat# ab40772
N-cadherin	Abcam	Cat# ab18203
Vimentin	Abcam	Cat# ab92547
CD133	Abcam	Cat# ab216323
SOX2	Abcam	Cat# ab97959
CD44	Abcam	Cat# ab157107
WDR66	Abcam	Cat# ab175369
E2F7	Abcam	Cat# ab245655
IGF2BP1	Abcam	Cat# ab184305
Rabbit IgG	Abcam	Cat# ab172730
Goat Anti-Rabbit IgG H&L (HRP)	Abcam	Cat# ab205718
Ago2	Abcam	Cat# ab186733
GAPDH	Abcam	Cat# ab8245
N-cadherin	Abcam	Cat# ab98952
Alexa Fluro 488-conjugated secondary antibody	Invitrogen	Cat# A11001
Alexa Fluro 594-conjugated secondary antibody	Invitrogen	Cat# A11012
Bacterial and virus strains		
Lentiviral pLKO.1 vector	Addgene	Cat# 8453
pLenti-EF1A-EGFP-F2A-Puro vector	Biovector	N/A
Biological samples		
CRC tissues and adjacent non-tumorous tissues	the Third Xiangya Hospital of Central South University	N/A
Chemicals, peptides, and recombinant proteins		
Actinomycin D	Sigma-Adrich	Cat# 50-76-0
RNase R	Epicenter Biotechnologies	Cat# RNR07250
5-fluorouracil	Sigma-Aldrich	Cat# 51-21-8
Critical commercial assays		
H&E staining Kit	Beyotime	Cat# C0105S
Lipofectamine 2000 Kit	Invitrogen	Cat# 11668019
PARIS Kit	Invitrogen	Cat# AM1921
Fluorescent *in Situ* Hybridization Kit	RiboBio	Cat# C10910
CCK-8 Kit	Beyotime	Cat# C0038
Cell-Light EdU Apollo567 *in vitro* Kit	RiboBio	Cat# C10310-1
ProLong Gold Antifade Mountant with DAPI Kit	Invitrogen	Cat# P36941
Annexin V Apoptosis Detection Kit	Invitrogen	Cat# V13242
PrimeScript RT Reagent Kit	TaKaRa	Cat# RR047A
miRNA 1st Strand cDNA Synthesis Kit	Vazyme	Cat# MR101-01
SYBR Green PCR Kit	Vazyme	Cat# Q111-02

(*Continued on next page*)

Continued

REAGENT or RESOURCE	SOURCE	IDENTIFIER
Pierce Bradford protein assay Kit	Thermo Fisher Scientific	Cat# 23200
Pierce ECL Plus Western Blotting Substrate Kit	Thermo Fisher Scientific	Cat# 32134
EZ-Magna RIP Kit	Millipore	Cat# 17-701
Pierce RNA pull-down Kit	Thermo Fisher Scientific	Cat# 20164
Dual luciferase reporter assay system Kit	Promega	Cat# E1910
Pierce magnetic ChIP Kit	Thermo Fisher Scientific	Cat# 26157
Deposited data		
UCSC	N/A	https://genome.ucsc.edu/
JASPAR	N/A	https://jaspar.genereg.net/
Starbase	N/A	https://rnasysu.com/encori/
Circinteractome	N/A	https://circinteractome.nia.nih.gov/
Experimental models: Cell lines		
SW480	ATCC	Cat# CCL-228
HCT116	ATCC	Cat# CCL-247
FHC	ATCC	Cat# CRL-1831
LoVo	ATCC	Cat# CCL-229
HT29	ATCC	Cat# HTB-38
SW620	ATCC	Cat# CCL-227
Experimental models: Organisms/strains		
Female BALB/c nude mice	Hunan SJA laboratory animal Co., Ltd	N/A
Oligonucleotides		
Sequences of miR-653-5p mimics/inhibitor, and their NC, see supplementary files	GeneChem	N/A
Sequences of shRNAs, see supplementary files	GeneChem	N/A
Primers for qRT-PCR, see STAR methods	Sangon Biotech	N/A
Recombinant DNA		
pcDNA3.1-E2F7	GeneChem	N/A
pcDNA3.1-IGF2BP1	GeneChem	N/A
pcDNA3.1-WDR66	GeneChem	N/A
pcDNA3.1-BMI1	GeneChem	N/A
pcDNA3.1 CircRNA mini vector	Addgene	Cat# 60648
pmirGLO vector	Promega	Cat# E1330
pGL3 Promoter vector	Promega	Cat# E1761
Software and algorithms		
ImageJ	N/A	N/A
GraphPad Prism software 7.0	GraphPad	https://www.graphpad.com/

RESOURCE AVAILABILLITY

Lead contact

Further information and request for resources and reagents should be directed to and will be fulfilled by the lead contact, Gui Hu (hugui22@csu.edu.cn).

Materials availability

Plasmids generated in this study: CircPOFUT1 was cloned into pcDNA3.1 CircRNA mini vector (Addgene, Watertown, MA, USA). For stable transfection, shRNAs against circPOFUT1 were cloned into lentiviral pLKO.1 vector (Addgene). CircPOFUT1 was cloned

into pLenti-EF1A-EGFP-F2A-Puro vector (Biovector), which is in detail described in the "STAR methods". The plasmids are available from the lead contact with a completed Materials Transfer Agreement.

Data and code availability

- All data reported in this paper will be shared by the lead contact upon request.
- This paper does not report original code.
- Any additional information required to reanalyze the data reported in this paper is available from the lead contact upon request.

EXPERIMENTAL MODEL AND STUDY PARTICIPANT DETAILS

Animals

All animal experiments were conducted with the approval of the Department of Laboratory Animals of Central South University (Changsha, Hunan, China) (No. CSU-2022-01-0057) and complied with the National Institutes of Health Guide for the Care and Use of Laboratory Animals. Female BALB/c nude mice (4-week-old) were used in this study. All mice have free access to standard chow and water under controlled temperature and constant 12 h/12 h light/dark cycles.

Clinical specimens

A cohort of 80 CRC tissues (Stage I n = 30; Stage II n = 25; Stage III+IV n = 25) and adjacent non-tumorous tissues were collected from patients with CRC at the Third Xiangya Hospital of Central South University. Diagnoses were confirmed by pathological analyses. Written consents were obtained from all patients. This study was approved by the Ethics Committee of the Third Xiangya Hospital of Central South University (No.2022-S472). The clinicopathological characteristics of CRC patients enrolled in the study were included in Table 1.

Cells

Normal colon cell line FHC and CRC cell lines LoVo, HT29, HCT116, SW480 and SW620 were from American Type Culture Collection (ATCC, Manassas, VA, USA). All the cell lines included in this study have been authenticated by STR profiling and tested for mycoplasma contamination. FHC cells were cultured in DMEM/F12 containing 10 ng/mL cholera toxin, 25 mM HEPES, 5 μg/mL transferrin, 5 μg/mL insulin, 100 ng/mL hydrocortisone and 10% FBS. CRC cell lines were grown in RPMI1640 supplemented with 10% FBS, and maintained at 37°C in 5% CO_2. All the medium and supplements were from Gibco (Grand Island, NY, USA).

METHOD DETAILS

Animal study and H&E staining

Female BALB/c nude mice (4-week-old, n = 6 per group) were obtained from SJA Laboratory Animal (Hunan, China). For the xenograft model, SW480 cells or HCT116 cells stably expressing sh-circPOFUT1 or circPOFUT1 were injected into the right flank of mice. Tumor volumes were measured every 5 days, and tumors were harvested and weighed on day 25. *In vivo* liver metastasis model was established as previous study described.[33] More precisely, SW480 cells (2×10^6 cells in 0.1 mL of PBS) were injected into the tail vein of mice. After 30 days, mice were sacrificed. For intra-splenic injection, mice were anesthetized, and the spleen was exposed. SW480 cells (3×10^6 cells in 0.05 mL of PBS) were slowly injected into the spleen.[34] The hepatic tissues were harvested and fixed with Bouin's solution (Sigma-Aldrich, St. Louis, MO, USA) and subjected to H&E staining according to the protocol from ref.[35] Specifically, hepatic tissues were embedded in paraffin and sliced into 5 μm sections. Sections were deparaffinized with xylene, and rehydrated in a series of decreasing alcohol concentrations. Hematoxylin staining for 5 min was used to visualize the nuclei, and then eosin staining for 3 min was used to highlight the cytoplasm. The liver metastatic nodules caused by tail vein or intra-splenic injection were lastly counted. All animal experiments were conducted with the approval of the Department of Laboratory Animals of Central South University (Changsha, Hunan, China) (No. CSU-2022-01-0057) and complied with the National Institutes of Health Guide for the Care and Use of Laboratory Animals.

Cell culture and treatment

Normal colon cell line FHC and CRC cell lines LoVo, HT29, HCT116, SW480 and SW620 were from American Type Culture Collection (ATCC, Manassas, VA, USA). FHC cells were cultured in DMEM/F12 containing 10 ng/mL cholera toxin, 25 mM HEPES, 5 μg/mL transferrin, 5 μg/mL insulin, 100 ng/mL hydrocortisone and 10% FBS. CRC cell lines were grown in RPMI1640 supplemented with 10% FBS, and maintained at 37°C in 5% CO_2. All the medium and supplements were from Gibco (Grand Island, NY, USA). To study the chemoresistance of CRC cells, SW480 and HCT116 cells were treated with designated doses of 5-fluorouracil (5-Fu, Sigma-Aldrich) for 24 h. For RNA stability assay, cells were incubated with vehicle control (PBS) or actinomycin D (2 μg/mL, Sigma-Aldrich) for 4, 8, 12 and 24 h. For RNase R digestion, total RNA (2 μg) was incubated with RNase R (Epicentre biotechnologies, Madison, WI, USA) at 37°C for 30 min. The expression of circPOFUT1 and POFUT1 were determined by qRT-PCR.

Plasmid construction and transfection

Mimics control (mimics NC), miR-653-5p mimics, inhibitor control (inhibitor NC), miR-653-5p inhibitor, scramble shRNA (sh-NC), sh-circPOFUT1#1, sh-circPOFUT1#2, sh-E2F7, sh-IGF2BP1, sh-WDR66 and sh-BMI1 were purchased from GeneChem (Shanghai, China). pcDNA3.1-E2F7, pcDNA3.1-IGF2BP1, pcDNA3.1-WDR66 and pcDNA3.1-BMI1 were also constructed by GeneChem. CircPOFUT1 was cloned into pcDNA3.1 CircRNA mini vector (Addgene, Watertown, MA, USA). For stable transfection, shRNAs against circPOFUT1 were cloned into lentiviral pLKO.1 vector (Addgene). CircPOFUT1 was cloned into pLenti-EF1A-EGFP-F2A-Puro vector (Biovector). pLKO.1-sh-circPOFUT1/pLenti-circPOFUT1, envelop and packaging vectors was transfected into HEK293 cells using Lipofectamine 2000 (Invitrogen). At 48 h post-transfection, viral supernatant was harvested and filtered. SW480 or HCT116 cells were transduced with circPOFUT1-knockdown or circPOFUT1-overexpressing lentiviral particles, respectively. SW480 and HCT116 cells were transfected with miRNA, shRNA and/or overexpression vector using Lipofectamine 2000 (Invitrogen, Carlsbad, CA, USA) according to the manufacturer's instructions. Stable cell line was established in the presence of puromycin (Invitrogen). Sequences of miR-653-5p mimics/inhibitor and their NC, and sequences of shRNAs were showed in supplemental files.

Subcellular fractionation

Subcellular fractionation was conducted using PARIS Kit (Invitrogen). In brief, cells were harvested and lysed with cell fractionation buffer. After centrifugation, the supernatants (cytoplasmic lysates) were collected, and the pellets (nuclear lysates) were lysed with cell disruption buffer. Both lysates were then subject to RNA isolation. U6 and GAPDH were used as the nuclear and cytoplasmic markers, respectively. The subcellular expression of circPOFUT1 was analyzed by qRT-PCR.

RNA Fluorescence *in situ* hybridization (FISH)

The circPOFUT1-Cy5 and miR-635-5p-FITC probes were synthesized by RiboBio (Guangzhou, China). RNA FISH was carried out using the Fluorescent *in Situ* Hybridization Kit (RiboBio). The subcellular localization of circPOFUT1 was visualized using a confocal microscope (Zeiss, Jena, Germany).

Cell proliferation assay

Cell counting kit-8 (CCK-8) assay was employed to monitor cell proliferation. Briefly, SW480 and HCT116 cells (1×10^3) were seeded into 96-well plates. At 1, 2, and 3 days post-transfection, CCK-8 solution (Beyotime, Shanghai, China) was added into each well. After incubation at 37°C for 1 h, the absorbance at 450 nm was measured using a microplate reader (BioTek, Winooski, VT, USA).

EdU incorporation assay

EdU incorporation assay was conducted using Cell-Light EdU Apollo567 *in vitro* Kit (Ribobio). Briefly, SW480 and HCT116 cells were incubated with EdU for 12 h. Cells were then fixed with 4% paraformaldehyde (PFA) and permeabilized with 0.5% Triton X-100, followed by the incubation with Apollo reaction cocktail. Nuclei were visualized by DAPI. Images were photographed using a confocal microscope (Zeiss).

Colony formation assay

SW480 and HCT116 cells (500 cells/per well) were seeded into 6-well plates and cultured for 14 days. Colonies were fixed in methanol and stained with crystal violet. The stained colonies were then photographed and counted using a light microscope (Olympus).

Transwell migration and invasion assays

Transwell assays were performed as described.[36] Specifically, for invasion assay, transfected cells were reseeded in Matrigel (Corning, Corning, NY, USA) coated upper Transwell chambers (Corning) and cultured in serum-free medium. The lower chambers were filled with RPMI1640 containing 10% FBS. Transwell migration assay was conducted without Matrigel coating. After 24 h, the invaded or migrated cells were fixed with 4% PFA and stained with crystal violet. The stained cells were then photographed and counted using a microscope (Olympus).

Immunofluorescence assay

SW480 and HCT116 cells were fixed with 4% PFA and permeabilized with 0.1% Triton X-100. After blocking with 10% normal goat serum, the cells were then incubated with anti-E-cadherin (1:200, ab40772, Abcam, Cambridge, UK) or anti-N-cadherin (1:200, ab98952, Abcam) antibody at 4°C overnight. Thereafter, cells were incubated with Alexa Fluro 488 or 594-conjugated secondary antibodies (2 μg/mL, A11001 or A11012, Invitrogen) and mounted in ProLong Gold Antifade Mountant with DAPI (Invitrogen). Images were photographed using a confocal microscope (Zeiss).

Flow cytometry assay

Cell apoptosis was monitored using Annexin V Apoptosis Detection Kit (Invitrogen). In brief, transfected cells were resuspended in binding buffer and incubated with Annexin V-FITC solution. Cells were then stained with PI and subjected to flow cytometry analysis (BD Biosciences, Franklin Lakes, NJ, USA).

Sphere formation assay

SW480 and HCT116 cells (1×10^3 per well) were plated into ultra-low attachment culture dishes (Corning), and cultured in RPMI1640 containing 20 ng/mL EGF, 20 ng/mL b-FGF, 2% B-27 and 1% N-2 supplement (Gibco).[37] After 14 days, the spheroid colonies were photographed and counted under a microscope (Olympus).

qRT-PCR

Total RNA was isolated using Trizol reagent (Invitrogen). For mRNA and circRNA, cDNA was synthesized using PrimeScript RT Reagent Kit (TaKaRa, Dalian, China) or miRNA 1st Strand cDNA Synthesis Kit (Vazyme, Nanjing, China), and qRT-PCR was conducted using SYBR Green PCR Kit (Vazyme). GAPDH or U6 was served as an internal control. The target gene expression was analyzed using $2^{-\Delta\Delta Ct}$ method. The primers used in this study were purchased from Sangon Biotech (Shanghai, China). To confirm the "head-to-tail" back-splicing of circPOFUT1, PCR was performed and products cloned into pGEM-T Easy vector were subjected to Sanger sequencing. Primers used in this study as follows:

CircPOFUT1-F: 5′-TGGCCCATTCTGGGATCAGT-3′;
CircPOFUT1-R: 5′-CTCCAAGCTGATGACCCGAT-3′;
POFUT1-F: 5′-ACCAGGCCGATCACTTCTTG-3′;
POFUT1-R: 5′-TCCAAGCTGATGACCCGATG-3′;
MiR-1197-RT: 5′-GTCGTATCCAGTGCAGGGTCCGAGGTATTCGCACTGGATACGACAGAAG T-3′;
MiR-1197-F: 5′-GCCGAGTAGGACACATGGTCT-3′;
MiR-1252-5p-RT: 5′-GTCGTATCCAGTGCAGGGTCCGAGGTATTCGCACTGGATACGACTAA ATG-3′;
MiR-1252-5p-F: 5′-GCCGAGAGAAGGAAATTGAATT-3′;
MiR-136-5p-RT: 5′-GTCGTATCCAGTGCAGGGTCCGAGGTATTCGCACTGGATACGACTCCA TC-3′;
MiR-136-5p-F: 5′-GCGGCACTCCATTTGTTTTGAT-3′;
MiR-149-5p-RT: 5′-GTCGTATCCAGTGCAGGGTCCGAGGTATTCGCACTGGATACGACGGGA GT-3′;
MiR-149-5P-F: 5′-CGTCTGGCTCCGTGTCTTC-3′;
MiR-653-5p-RT: 5′-GTCGTATCCAGTGCAGGGTCCGAGGTATTCGCACTGGATACGACCAGT AG-3′;
MiR-653-5p-F: 5′-GCCGAGGTGTTGAAACAATCT-3′;
E2F7-F: 5′-CAGGCAGCCCAGACTAGATT-3′;
E2F7-R: 5′-CAGGTTAGCTGTGGGTGTCC-3′;
WDR66-F: 5′-TCCTATGATGGCTGCTACGC-3′;
WDR66-R: 5′-GCTTCTTGATGTGTCTGATGGG-3′;
BMI1-F: 5′-GACTCTGGGAGTGACAAGGC-3′;
BMI1-R: 5′-AGATTGGTGGTTACCGCTGG-3′;
GAPDH-F: 5′-CTGACTTCAACAGCGACACC-3′;
GAPDH-R: 5′-GTGGTCCAGGGGTCTTACTC-3′;
U6-F: 5′-CTCGCTTCGGCAGCACA-3′;
U6-R: 5′-AACGCTTCACGAATTTGCGT-3′.

Western blot

Protein lysates were prepared using RIPA lysis buffer supplemented with protease inhibitor (Roche, Mannheim, Germany). Protein concentration estimation was performed using Bradford protein assay (Thermo Fisher Scientific). Proteins were separated by SDS-PAGE and transferred onto PVDF membranes. The blots were then subjected to blocking and incubation with primary antibodies. Thereafter, the blots were incubated with corresponding secondary antibodies. The signals were visualized using Pierce ECL Plus Western Blotting Substrate (Thermo Fisher Scientific). Antibodies used in Western blot were: anti-E-cadherin (1:2000, ab40772, Abcam), anti-N-cadherin (1:1000, ab18203, Abcam), anti-Vimentin (1:1000, ab92547, Abcam), anti-CD133 (1:1000, ab216323, Abcam), anti-SOX2 (1:1000, ab97959, Abcam), anti-CD44 (1:1000, ab157107, Abcam), anti-WDR66 (1:1000, ab175369, Abcam), anti-E2F7 (1:1000, ab245655, Abcam) and anti-GAPDH (1:1000, ab8245, Abcam).

RNA pull-down assay

RNA pull-down assay was conducted using Pierce RNA pull-down Kit (Thermo Fisher Scientific). In brief, oligo probe (negative control) or circPOFUT1/miR-635-5p probe was conjugated with streptavidin beads and incubated with cell lysates. RNA was extracted using Trizol reagent, and subjected to qRT-PCR analysis.

Dual luciferase reporter assay

The wild-type or mutated 3′UTR of E2F7 (E2F7-WT or E2F7-MUT) was cloned into pmirGLO vector (Promega, Madison, WI, USA). The promoter region of WDR66 (869–882) was cloned into pGL3 Promoter vector (Promega). HEK293 cells were co-transfected with miRNAs/shRNAs/overexpression construct and corresponding luciferase constructs. Relative luciferase activity was measured using Dual luciferase reporter assay system (Promega). Renilla luciferase acted as an internal control.

RNA immunoprecipitation (RIP) assay

RIP was conducted using Magna RIP Kit (Millipore, Billerica, MA, USA). Briefly, antibody against Ago2 (ab186733, Abcam), IGF2BP1 (ab184305, Abcam) or normal IgG conjugated beads were incubated with cell lysates at 4°C overnight. The enriched circPOFUT1, E2F7 mRNA and miR-635-5p were detected by qRT-PCR.

Chromatin immunoprecipitation (ChIP) assay

ChIP assay was performed using Pierce magnetic ChIP Kit (Thermo Fisher Scientific). Briefly, cells were cross-linked with 1% formaldehyde, and chromatin fractions were prepared by MNase (Thermo Fisher Scientific) digestion. Antibody against E2F7 (ab245655, Abcam) or normal IgG conjugated beads were incubated with chromatin fractions, followed by DNA purification and qPCR analysis.

QUANTIFICATION AND STATISTICAL ANALYSIS

All experiments were performed in at least three biological replicates, and each biological replicate contained three technical replicates. GraphPad Prism Software 7.0 (GraphPad, San Diego, CA, USA) was employed for statistical analysis. All the data meet the assumption of normal distribution. Student's *t* test was used to analyze differences between two groups. One-way analysis of variance (ANOVA) followed by Tukey's post hoc test was used to analyze differences among multiple groups. Survival curve was calculated using the Kaplan-Meier analysis. $p < 0.05$ was considered to be statistically significant.